CONFIDENTIAL

NACA RM L53I28a

NACA

RESEARCH MEMORANDUM

AERODYNAMIC CHARACTERISTICS OF A CANARD-BALANCED, FREE-FLOATING, ALL-MOVABLE STABILIZER AS OBTAINED FROM ROCKET-POWERED-MODEL FLIGHT TESTS AND LOW-SPEED WIND-TUNNEL TESTS

By William N. Gardner

Langley Aeronautical Laboratory
Langley Field, Va.

NATIONAL ADVISORY COMMITTEE
FOR AERONAUTICS

WASHINGTON

December 4, 1953

CONFIDENTIAL

NATIONAL ADVISORY COMMITTEE FOR AERONAUTICS

RESEARCH MEMORANDUM

AERODYNAMIC CHARACTERISTICS OF A CANARD-BALANCED, FREE-FLOATING, ALL-MOVABLE STABILIZER AS OBTAINED FROM ROCKET-POWERED-MODEL FLIGHT TESTS AND LOW-SPEED WIND-TUNNEL TESTS

By William N. Gardner

SUMMARY

Low-speed wind-tunnel tests and flight tests at Mach numbers from 0.6 to 1.46 were conducted on two rocket-powered research models incorporating a proposed all-movable-type horizontal tail. The free-floating tail consists of a delta-surface stabilizer with a linked-trailing-edge flap. Mounted forward of the stabilizer on a boom is a canard-type delta-surface servoplane which acts as the control in trimming the free-floating tail to produce the desired lift.

The results obtained from these tests indicate that servoplane downwash effects on the free-floating stabilizer are overbalancing, particularly at high angles of attack, and that servoplane effectiveness changes only slightly as Mach number increases. The tendency of the free-floating tail to float into the wind is quite low at subsonic speeds but increases rapidly in the transonic range and decreases with increasing angle of attack. In the transonic range, the tail hinge moments due to angle of attack increase rapidly, whereas the hinge moments due to flap deflection decrease, the combined result being an irregular but comparatively steady value of hinge moment per unit tail deflection. The sum of the tail damping derivatives is constant with Mach number except over a narrow range at Mach number 0.98 where the tail is dynamically unstable. The maneuvering effectiveness of the all-movable tail is consistently quite high over the Mach number range of these tests, and the linked flap is satisfactory in allowing the tail to provide static stability to the complete configuration. Above a Mach number of 0.95 there is a steadily increasing positive tail trim change which results from a change in the tail trim hinge moment. Interference effects of the vertical tail and the horizontal- and vertical-tail juncture are believed to be responsible for this trim change.

INTRODUCTION

The advent of transonic and supersonic airplanes has greatly increased the necessity for designing control systems which are capable of overcoming the serious trim, stability, control hinge moment, and control effectiveness changes which occur throughout the complete speed range from low subsonic to supersonic speeds. The advantages of an all-movable-type control as compared to a flap-type control have been known for some time. Some of these advantages are noted in reference 1. Previous work on all-movable controls such as that reported in references 2 to 5 indicates the practicality of their use on airplanes. Reference 4 concludes that, although an all-movable horizontal tail would be expected to offer improved elevator-control characteristics at high subsonic speeds as compared to a conventional elevator control, a power boost system would still be required at Mach numbers near unity to overcome the high stick forces resulting from rearward movement of the tail center of pressure. Later work with an all-movable horizontal tail reported in reference 5 indicates that, by using a mechanical system which allows the linked unbalancing flap employed on the tail to serve both as a linked and servo flap, satisfactory control characteristics can be achieved in both rapid and steady maneuvers while maintaining near-zero values of tail hinge-moment variation with deflection and angle of attack. Again, however, rearward movement of the tail center of pressure and loss of servo flap effectiveness would result in high stick forces at sonic speeds.

Recently, a somewhat different type of all-movable horizontal tail has been proposed by the Grumman Aircraft Engineering Company (GAEC) for use in the transonic- and supersonic-speed ranges. The proposed tail is unique in that it is free floating and utilizes an aerodynamic-type servo for positioning. The purpose of the tail is, of course, to provide a longitudinal stabilizing and control system which will have satisfactory handling characteristics throughout the speed range without the use of any mechanical power boost in the pilot's control system. The pilot's control would be directly connected to the aerodynamic servo. The free-floating horizontal tail consists of a delta-surface stabilizer having a linked unbalancing trailing-edge flap. Mounted forward of the stabilizer on a boom is a canard-type delta-surface servoplane which acts as the control surface in trimming the tail to produce the desired lift. The purpose of the linked flap is to allow the tail to provide a static-stability contribution to a configuration on which it might be employed.

In this tail design an effort has been made to take advantage of the rearward shift in center of pressure of the delta-surface stabilizer and loss of effectiveness of the linked unbalancing flap at transonic speeds. The rearward shift of the stabilizer center of pressure counteracts the loss in unbalancing flap effectiveness so that the net result will be a nearly constant value of the tail hinge-moment derivative due

to tail deflection throughout the speed range. Such an arrangement would allow the use of a canard-type aerodynamic servo.

Two rocket-model tests and low-speed wind-tunnel tests have been made to determine the hinge-moment, damping, lift, and trim characteristics of this proposed horizontal tail and the effectiveness of the aerodynamic servo. The low-speed wind-tunnel tests were preliminary in nature and served to allow closer estimation of necessary control-deflection limits and rocket-model instrument ranges. In these tests the free-floating horizontal tail is mounted on the tip of a swept vertical tail. This tail arrangement was mounted on a cylindrical-body rocket-powered test vehicle. Throughout the flight tests, the canard servoplane was pulsed in a square-wave manner and the responses of the model and tail were observed. In the wind-tunnel tests the trim tail deflection was recorded over a range of angle of attack for various settings of the servoplane.

SYMBOLS

Figure 1 is a schematic drawing of the rocket-model and free-floating horizontal tail which is presented as an aid in defining the applicable symbols and their sign convention. All the coefficient and derivative data presented in this paper are based on the stabilizer area and mean aerodynamic chord and have the dimension per degree. Whenever a dot is used above a symbol, it denotes differentiation with respect to time.

α	angle of attack, deg
θ	angle of pitch, deg
γ	flight-path angle, deg
δ	horizontal-tail deflection, deg
δ_c	servoplane deflection, deg
δ_f	flap deflection, deg
ϵ	servoplane downwash angle, deg
r	flap linkage ratio, δ_f/δ
f	frequency, cps
S	stabilizer area, sq ft

$\bar{c}$	stabilizer mean aerodynamic chord, ft
q	dynamic pressure, lb/sq ft
V	velocity, ft/sec
M	Mach number
R	Reynolds number, based on stabilizer mean aerodynamic chord
$T_{1/2}$	time to damp to one-half amplitude, sec
m	mass, slugs
I_Y	moment of inertia of complete model about pitch axis, slug-feet^2
I_{Y_t}	moment of inertia of horizontal tail about pivot axis, slug-feet^2
C_L	lift coefficient
C_{L_o}	lift coefficient at α, δ, and $\delta_c = 0$
C_m	model pitching-moment coefficient about model center of gravity
C_{m_o}	model pitching-moment coefficient at α, δ, and $\delta_c = 0$
C_h	hinge-moment coefficient
C_{h_o}	tail hinge-moment coefficient at α, δ, and $\delta_c = 0$

Lift derivatives:

C_{L_α}	rate of change of model lift coefficient with angle of attack when tail is free
C_{L_α}'	rate of change of model lift coefficient with angle of attack when tail is fixed
C_{L_δ}	rate of change of model lift coefficient with tail deflection when flap is linked
$C_{L_{\delta_c}}$	rate of change of model lift coefficient with servoplane deflection

$C_{L_{\delta_f}}$ rate of change of tail lift coefficient with flap deflection

$\left(C_{L_b}\right)_\alpha$ rate of change of fuselage lift coefficient with angle of attack

$\left(C_{L_t}\right)_\alpha$ rate of change of tail lift coefficient with angle of attack

$\left(C_{L_t}\right)_\delta$ rate of change of tail lift coefficient with tail deflection when flap is fixed

$\left(C_{L_s}\right)_\delta$ rate of change of tail lift coefficient due to stabilizer with tail deflection when flap is fixed

$\left(C_{L_c}\right)_\delta$ rate of change of tail lift coefficient due to servoplane with tail deflection

$\left(C_{L_c}\right)_{\delta_c}$ rate of change of tail lift coefficient due to servoplane with servoplane deflection

Pitching-moment derivatives:

C_{m_α}' rate of change of model pitching-moment coefficient with angle of attack when tail is fixed

C_{m_δ} rate of change of model pitching-moment coefficient with tail deflection

$C_{m_{\delta_c}}$ rate of change of model pitching-moment coefficient with servoplane deflection

$C_{m_{\dot{\alpha}}}$ rate of change of model pitching-moment coefficient with rate of change of angle of attack, $\frac{\partial C_m}{\partial \frac{\dot{\alpha}\bar{c}}{2V}}$

$C_{m_{\dot{\theta}}}$ rate of change of model pitching-moment coefficient with rate of change of angle of pitch, $\frac{\partial C_m}{\partial \frac{\dot{\theta}\bar{c}}{2V}}$

Hinge-moment derivatives:

C_{h_α} rate of change of tail hinge-moment coefficient with angle of attack

C_{h_δ} rate of change of tail hinge-moment coefficient with tail deflection

$C_{h_{\delta_c}}$ rate of change of tail hinge-moment coefficient with servoplane deflection

$C_{h_{\delta_f}}$ rate of change of tail hinge-moment coefficient with flap deflection

$\left(C_{h_s}\right)_\alpha$ rate of change of tail hinge-moment coefficient due to stabilizer with angle of attack when flap is fixed

$\left(C_{h_c}\right)_\alpha$ rate of change of tail hinge-moment coefficient due to servoplane with angle of attack

$\left(C_{h_{fH}}\right)_\alpha$ rate of change of tail hinge-moment coefficient due to flap hinge moments with angle of attack

$\left(C_{h_c}\right)_\delta$ rate of change of tail hinge-moment coefficient due to servoplane with tail deflection

$\left(C_{h_c}\right)_{\delta_c}$ rate of change of tail hinge-moment coefficient due to servoplane with servoplane deflection

$\left(C_{h_{fL}}\right)_{\delta_f}$ rate of change of tail hinge-moment coefficient due to flap lift forces with flap deflection

$\left(C_{h_{fH}}\right)_{\delta_f}$ rate of change of tail hinge-moment coefficient due to flap hinge moments with flap deflection

$C_{h_{\dot\theta}}$ rate of change of tail hinge-moment coefficient with rate of change of angle of pitch, $\dfrac{\partial C_h}{\partial \dfrac{\dot\theta \bar c}{2V}}$

$C_{h_{\dot\alpha}}$ rate of change of tail hinge-moment coefficient with rate of change of angle of attack, $\dfrac{\partial C_h}{\partial \dfrac{\dot\alpha \bar c}{2V}}$

$C_{h_{\dot\delta}}$ rate of change of tail hinge-moment coefficient with rate of change of tail deflection, $\dfrac{\partial C_h}{\partial \dfrac{\dot\delta \bar c}{2V}}$

Subscripts:

b	fuselage
c	servoplane
f	flap
s	stabilizer
t	horizontal tail

MODELS, INSTRUMENTATION, AND TESTS

Rocket Models

Configuration.- A drawing of the complete test vehicle is shown in figure 2(a) and a detail drawing of the horizontal tail unit is shown in figure 2(b). Figure 2(c) is a detail drawing of the horizontal tail and vertical fin intersection. Two models were flight tested. The second model was identical to the first model except for a body boattail fairing which was added to the second model. Figure 2(d) shows a detail drawing of this fairing. Photographs of the complete model are shown in figure 3.

The models consisted of a standard NACA rocket-model research vehicle which was modified to accommodate the proposed horizontal and vertical tail arrangement. The body nose ordinates may be found in reference 6. In order to balance the model and to insure minimum lateral motion, a ventral fin identical to the main vertical tail was added to the configuration. At the tip of this ventral fin was located a lead "tip tank" which served as a balancing ballast weight. The main vertical tail and the horizontal tail were machined magnesium castings, and the ventral fin was constructed of laminated wood with metal inserts. The geometric characteristics of the horizontal and vertical tails are listed in table I.

The horizontal-tail unit is mounted on a roller-bearing pivot at the tip of the vertical tail and within fixed limits is free floating about this pivot axis. A constant-chord flap on the stabilizer is linked in a 1:1 ratio through the pivot axis and functions as a leading or unbalancing tab. The servoplane, mounted forward of the stabilizer on a boom, is actuated by means of a pneumatic servomotor contained within the boom. Flexible air lines which offer no restraint to the stabilizer are provided through the pivot axis. All other components of the pneumatic system are contained within the body. Figure 4 is a top-view photograph of the horizontal tail with the boom hatch cover removed and shows the component parts of the horizontal tail and the servoplane pulsing motor.

Throughout the remainder of this report the first model will be referred to as Model A and the second as model B. Table II is a list of the mass characteristics of the two models.

Instrumentation.- Models A and B contained seven-channel telemeters transmitting measurements of normal and longitudinal acceleration, angle of attack, total pressure, a reference static pressure, stabilizer deflection, and servoplane deflection. Angle of attack was measured by a vane-type instrument located on the nose of the model (fig. 2(a)). In order to extend the positive angle-of-attack range of the instrument, the mounting sting was deflected down 5° with respect to the model center line. Total pressure was measured by a small pressure probe extending from the side of the body (fig. 2(a)), and static pressure was measured through an orifice in the body skin at a point on the cylindrical portion of the body near the ogive nose section. Longitudinal and normal accelerometers were placed in the leading edge of the dummy fin at the fin root which was near the model center of gravity. Stabilizer and servoplane deflections were measured by control-position pickups mounted in the fin and horizontal-tail boom, respectively.

CW Doppler radar and tracking radar units were used for obtaining additional data on model velocity and flight path. Atmospheric conditions were determined by radiosonde observations made shortly after each flight. Fixed and manually operated motion-picture cameras were used to photograph the launching and flight of each model.

Tests.- The models were boosted to a Mach number of 1.15 by 6-inch ABL Deacon rocket motors, and approximately $1\frac{1}{2}$ seconds after booster separation the 5-inch Cordite sustainer rocket motors were intended to fire and increase the speed to a maximum value of $M = 1.4$. The sustainer motor ignitor circuits in model A malfunctioned, and the sustainer motor did not fire until 27 seconds after booster separation. Thus, the maximum Mach number reached by the model was only $M = 1.2$. Model B performed as intended and reached a maximum Mach number of 1.46. The models were launched at angles of approximately 45° from the horizontal by means of a crutch-type launcher. Figure 5 is a photograph of model B in combination with its booster rocket mounted on the launching platform. In order to simplify the launching arrangement, the models were rolled 90° when mounted on the launcher. Flight tests of these models were conducted at the Langley Pilotless Aircraft Research Station at Wallops Island, Va.

Data on the characteristics of these models were obtained during the coasting parts of the flights following booster separation and sustainer burnout. The CW Doppler radar unit obtained velocity data on each model during and immediately after the boosted portion of the flights but failed to yield reliable data after this time. The tracking radar obtained flight-path data for both models throughout the entire flight. Mach numbers and dynamic pressures were, therefore, determined for both

models from the telemetered total and static pressures. Static pressure as determined by combining the tracking radar and radiosonde observations was used as a check on the telemeter data. The measured angle-of-attack and accelerometer data were corrected to angles and accelerations at the model centers of gravity. The approximate range of Reynolds numbers (based on the stabilizer mean aerodynamic chord) obtained during the flights is shown in figure 6 as a function of Mach number. All the coefficients and derivatives presented in this paper are based on the stabilizer area and mean aerodynamic chord.

The method of conducting these rocket-model tests was to pulse the servoplane in an approximate square-wave manner at a rate of one pulse every 1/2 second. The pulse rate was controlled by a motor-driven sequence valve. Set-screw-type stops were provided to limit the servoplane deflection on each model. On model A these stops were set at 1° and -2°, and on model B the stops were set at 0° and -3.7°. Design of the vertical- and horizontal-tail intersection limited the deflection range of the free-floating horizontal tail to 2° and -5°. From the transient oscillations of the tail after a pulse of the servoplane, the tail damping, hinge moments, and lift were determined. Servoplane effectiveness was determined from the change in trim of the tail after a pulse of the servoplane. In these tests the aerodynamic characteristics of the complete model are of minor importance, and the natural pitch frequency of the models was of the same order of magnitude as the servoplane pulse frequency. Consequently, the pitch oscillations of the models throughout these tests are random and have no significance as to the horizontal-tail effectiveness, model stability, or model damping. The floating characteristics of the free-floating tail as the model changes angle of attack, however, are significant of the tail trim characteristics and the relationship between the tail hinge moments due to angle of attack and those due to tail deflection.

Throughout the flight of model A the model oscillated generally in the low angle-of-attack range from -5° to 5°, being more in the negative range at low speeds and more in the positive range at high speeds. In the transonic-speed range the tail experienced a trim change which, in conjunction with an increased floating tendency, resulted in the tail either striking or remaining at its positive deflection limit for a large portion of the time at high speeds. This was particularly true at the 1° servoplane position. Thus, the transient oscillations of the tail were invalidated in many cases, and the amount of high-speed data obtained from the test was limited. Data presented in reference 6 indicate that a body boattail may influence the local flow over a horizontal tail mounted above the body. In order to eliminate any possible effect of the body boattail on the trim characteristics of the horizontal tail of model B, a fairing was added to the body (fig. 2(d)) which extended the cylindrical section of the body to the trailing edge of the horizontal tail.

Throughout the flight of model B the model oscillated generally in the angle-of-attack range from 0° to 10° as was intended by increasing the negative deflection range of the servoplane over that of model A. As in the case of model A, the trim changes and increased floating tendency of the horizontal tail resulted in the tail being on its stop for a large portion of the time at high transonic speed. However, in the test of model B the tail was on its negative stop rather than on the positive stop as on model A. Consequently, the amount of high-speed data obtained at the -3.7° servoplane deflection on model B was limited.

Wind-Tunnel Model

Figure 7 is a drawing showing the general arrangement of the wind-tunnel model, and figure 8 shows photographs of the model mounted in the Langley stability tunnel. In order to facilitate the wind-tunnel tests, rocket model A was modified for installation in the wind tunnel and no special model was necessary. Model A was modified by removing the fuselage power supply section and by removing the dummy vertical fin. Removing the fuselage power supply section shortened the fuselage nose sufficiently to prevent the nose of the model from striking the tunnel ceiling at high angles of attack. The model was mounted on the wind-tunnel support strut at the dummy fin fitting. As may be seen in the photographs of figure 8, an extension tube was attached to the rear of the body and a connecting link projected through the tunnel ceiling. This setup was used to change the angle of attack of the model during the wind-tunnel tests since it was not possible to use the wind-tunnel angle-of-attack system. A control position pickup was installed in the vertical fin to measure the deflection angles of the free-floating horizontal tail, and set screws were provided to adjust the position of the servoplane.

Two series of wind-tunnel tests were made in the Langley stability tunnel, one utilizing the original horizontal-tail configuration and the other utilizing a servoplane which was identical to the original configuration in plan form but having only 80 percent of the area of the original servoplane. Figure 9 is a detail drawing of the original and small servoplanes. The purpose of these wind-tunnel tests was to obtain an indication of servoplane effectiveness, horizontal-tail trim, and tail floating characteristics which could be used in determining satisfactory servoplane deflection limits and instrumentation limits for the rocket-model tests. The wind-tunnel tests were made at a dynamic pressure of 65 pounds per square foot which corresponded to a Mach number of 0.2 and a Reynolds number of 1.7×10^6 (based on the stabilizer mean aerodynamic chord).

In each of these two series of tests the trim position of the free-floating tail was measured as the angle of attack of the model and the deflection of the servoplane were varied. The range of the servoplane

settings was from -6° to 6°, and the angle-of-attack range was from -10° to 20°. As in the case of the rocket models the deflection range of the horizontal tail was limited to -5° and 2°. Additional tests were made with the servoplane removed. No corrections have been applied to the data obtained from these tests.

METHOD OF ANALYSIS

Derivation of Equations of Motion

All-movable-type control systems are not new. However, the control system discussed in this paper is unconventional in that it employs a freely floating stabilizer positioned by a canard-type aerodynamic servoplane. The free-floating stabilizer is held in partial restraint by the aerodynamic moments produced by a linked trailing-edge flap. The unique character of this control necessitates the derivation of unconventional equations of motion for analysis of the control system even though only fundamental aerodynamic principles are involved. In order to convey a more complete understanding of this control system and its components, as well as the significance of the data presented in this paper, simplified equations of motion for the system will be discussed here. Generalized equations of motion which might be applied to this control system may be found in reference 7.

By assuming a three-degree-of-freedom system involving deflection of the free-floating horizontal tail (pitching motion of the tail about the tail pivot axis), pitching motion of the complete model about the model center of gravity, and angle of attack of the complete model, the three simplified equations of motion are as follows:

$$C_{h_{\delta_c}}\delta_c = \frac{I_{Y_t}}{57.3qS\bar{c}}(\ddot{\theta} + \ddot{\delta}) - \frac{\bar{c}}{2V}C_{h_{\dot{\delta}}}(\dot{\theta} + \dot{\delta}) - \frac{\bar{c}}{2V}C_{h_{\dot{\alpha}}}(\dot{\alpha} + \dot{\delta}) - C_{h_\alpha}\alpha - C_{h_\delta}\delta - C_{h_o} \tag{1}$$

$$C_{m_{\delta_c}}\delta_c = \frac{I_Y}{57.3qS\bar{c}}\ddot{\theta} - \frac{\bar{c}}{2V}C_{m_{\dot{\theta}}}\dot{\theta} - \frac{\bar{c}}{2V}C_{m_{\dot{\alpha}}}\dot{\alpha} - C_{m_\alpha}{}'\alpha - C_{m_\delta}\delta - C_{m_o} \tag{2}$$

$$C_{L_{\delta_c}}\delta_c = \frac{mV}{57.3qS}\dot{\gamma} - C_{L_\alpha}{}'\alpha - C_{L_\delta}\delta - C_{L_o} \tag{3}$$

In these equations the terms resulting from the effects of apparent mass, body downwash, and the hinge-moment terms resulting from tail displacement from the model center of gravity have been neglected. The tail is

assumed to be mass-balanced about the pivot axis and the linked flap is assumed to be mass-balanced about its hinge line. The terms which would result from the fact that the linked flap is not dynamically balanced about the tail pivot axis have also been neglected.

Equation (1), which represents a summation of the hinge moments acting on the horizontal tail about the tail pivot axis, is the equation of least familiarity and of primary importance in this report. Equations (2) and (3) represent the pitching moments and lift forces, respectively, of the complete configuration and are of secondary importance in this paper. The moment and lift derivatives appearing in these equations are complex in nature and a detailed analysis of these derivatives is necessary.

The pivot axis of the horizontal-tail unit is located ahead of the tail aerodynamic center. Therefore, the tail unit is stable with respect to angle of attack and would, if unrestrained, maintain a constant angle of attack to the relative wind. In such a case the tail unit would provide a trimming moment but would be incapable of providing a stability or damping contribution to an airplane configuration on which it might be employed if friction and mass effects are neglected. The restraint necessary to realize an airplane stability and damping contribution of the tail is obtained by use of the linked trailing-edge flap which in the subject system is linked in a 1:1 ratio as a leading or unbalancing flap.

The control moment necessary to deflect the tail from its floating position to a desired trim deflection is obtained by deflecting the servoplane. The moment required to deflect the servoplane is in no way associated with the moment required to deflect the complete-tail unit since the servoplane actuating system is routed through the pivot axis in such a manner that no moment is transmitted to the tail unit. In the present tests, the moment required to deflect the servoplane has not been considered.

Hinge-moment derivatives.- Under all trim conditions the tail unit must be in aerodynamic equilibrium and the summation of hinge moments about the pivot axis is zero. For this case equation (1) becomes

$$C_{h_{\delta_c}}\delta_c + C_{h_\alpha}\alpha + C_{h_\delta}\delta + C_{h_o} = 0 \qquad (4)$$

For constant values of α, equation (4) may be differentiated with respect to δ_c to obtain the following relationship:

$$C_{h_{\delta_c}} = -\frac{d\delta}{d\delta_c} C_{h_\delta} \qquad (5)$$

which simply shows that the servoplane effectiveness, expressed as $d\delta/d\delta_c$, in deflecting the tail unit is directly proportional to the tail hinge-moment derivative about the pivot axis due to servoplane deflection and inversely proportional to the hinge-moment derivative due to tail deflection. The hinge-moment derivative $C_{h_{\delta_c}}$ represents the sum of the hinge moments about the pivot axis due to the lift force produced by deflecting the servoplane and the hinge moments resulting from servoplane downwash effects on the stabilizer and linked flap. Thus

$$C_{h_{\delta_c}} = \left(C_{h_c}\right)_{\delta_c} + \frac{d\epsilon}{d\delta_c}\left[\left(C_{h_s}\right)_\alpha + \left(C_{h_{fH}}\right)_\alpha\right] \tag{6}$$

Again in equation (4) for constant values of δ_c differentiation with respect to α yields the relationship

$$C_{h_\alpha} = -\frac{d\delta}{d\alpha} C_{h_\delta} \tag{7}$$

The term $d\delta/d\alpha$ is indicative of the tail floating characteristics as angle of attack is changed and is also a measure of the tail contribution to airplane stability and damping. A zero value of $d\delta/d\alpha$ indicates that the tail is functioning just as a fixed tail, while negative values indicate that the tail tends to float into the wind and positive values against the wind. Thus, a value of -1 would indicate a completely free floating tail which would make no contribution to airplane stability and damping. As indicated in equation (7), $d\delta/d\alpha$ is directly proportional to the tail hinge-moment derivative due to angle of attack and inversely proportional to the hinge-moment derivative due to tail deflection. The hinge-moment derivative C_{h_α} represents the tail hinge moments due to angle of attack and consists of the hinge moments resulting from the servoplane lift force, the stabilizer lift force, and the linked flap hinge-moment about the flap hinge line. Therefore,

$$C_{h_\alpha} = \left(C_{h_c}\right)_\alpha + \left(1 - \frac{d\epsilon}{d\alpha_t}\right)\left[\left(C_{h_s}\right)_\alpha + \left(C_{h_{fH}}\right)_\alpha\right] \tag{8}$$

In equation (8) the hinge moments produced by the stabilizer and flap are, of course, affected by the servoplane downwash angle as indicated. For all practical purposes the derivative $\left(C_{h_c}\right)_\alpha$ in equation (8) is equivalent to the derivative $\left(C_{h_c}\right)_{\delta_c}$ in equation (6) because the only difference in servoplane lift resulting from tail angle of attack

and that due to servoplane deflection is the difference in the interference effect between the servoplane and tail boom in the two cases. This difference in interference effects is believed to be negligible. Similarly the servoplane downwash factors, $d\epsilon/d\alpha_t$ in equation (8) and $d\epsilon/d\delta_c$ in equation (6), may be considered equivalent.

Insofar as the aerodynamic forces and moments on the tail are concerned there is no difference between the effects of angle of attack and of tail deflection with the exception of the linked flap and the interference effects of the vertical tail. Throughout this analysis the interference effects of the vertical tail on the horizontal tail will be neglected. Therefore, the hinge-moment derivative C_{h_δ} may be expressed as

$$C_{h_\delta} = C_{h_\alpha} + rC_{h_{\delta_f}} \tag{9}$$

The hinge-moment derivative due to flap deflection $C_{h_{\delta_f}}$ represents the sum of the hinge moments about the pivot axis resulting from the flap lift force and from the flap hinge moment about the flap hinge line. Consequently, the derivative $C_{h_{\delta_f}}$ may be expressed as

$$C_{h_{\delta_f}} = \left(C_{h_{fL}}\right)_{\delta_f} + \left(C_{h_{fH}}\right)_{\delta_f} \tag{10}$$

Since all the static hinge-moment derivatives which occur in equation (1) have been considered, the dynamic derivatives will now be discussed. Since the control system discussed here is free-floating, the damping characteristics of the tail are of vital importance. The tail damping moments arise from two sources which are the lag in downwash on the tail and the rotary motion of the tail. The tail angle of attack is equal to $\alpha + \delta$, and the rate of change of the tail angle of attack is equal to $\dot{\alpha} + \dot{\delta}$. Therefore, the tail damping moment arising from the lag in downwash on the tail may be expressed, as in equation (1), by

$$\frac{\bar{c}}{2V} C_{h_{\dot{\alpha}}}\dot{\alpha} + \frac{\bar{c}}{2V} C_{h_{\dot{\alpha}}}\dot{\delta}$$

Similarly, the rotary motion of the tail is equal to $\dot{\theta} + \dot{\delta}$ and the tail damping moment due to rotary motion may be expressed, as in equation (1), by

$$\frac{\bar{c}}{2V} C_{h_{\dot{\delta}}}\dot{\theta} + \frac{\bar{c}}{2V} C_{h_{\dot{\delta}}}\dot{\delta}$$

The derivative $C_{h_{\dot{\delta}}}$ as used in the rotary damping expression is assumed to be equivalent to the derivative $C_{h_{\dot{\theta}}}$ since, as previously assumed, the interference effect of the vertical tail on the horizontal tail has been neglected. This same circumstance exists in the previous case where the derivative $C_{h_{\dot{\alpha}}}$ is used in conjunction with $\dot{\delta}$.

Pitching-moment derivatives.- The nature of the present investigation is such that no pitching-moment data were obtained, and the pitching-moment derivatives will not be analyzed here. Pitching-moment data on the configuration of these tests would not be of any particular importance. It should perhaps be pointed out that the primary contribution of the tail to configuration pitching moment arises from the tail lift, but there is also a small contribution of the linked flap which is independent of tail lift. The flap hinge moment is transferred to the configuration through the flap linkage as a pitching moment.

Lift derivatives.- Equation (3), which represents a summation of the lift forces acting on the complete configuration, contains at least one term which requires detailed explanation. This term, C_{L_α}', which is the lift derivative due to angle of attack when the tail is considered fixed, differs in the present case from the conventional lift derivative C_{L_α} in that the tail is normally free floating with controls fixed. In a conventional control system δ is fixed when the stick is fixed; however, in the present system, fixing the stick only fixes the servoplane and does not fix δ. Therefore,

$$C_{L_\alpha}' = \left(C_{L_b}\right)_\alpha + \left(C_{L_t}\right)_\alpha \tag{11}$$

where the tail lift derivative $\left(C_{L_t}\right)_\alpha$, on the basis of the previously stated fin-interference assumption, is assumed to be equivalent to the derivative $\left(C_{L_t}\right)_\delta$, and

$$\left(C_{L_t}\right)_\delta = \left(C_{L_c}\right)_\delta + \left(1 - \frac{d\epsilon}{d\delta}\right)\left(C_{L_s}\right)_\delta \tag{12}$$

In defining C_{L_α}, the conventional lift derivative, as it is applied in the present case, the floating characteristics (or the ratio of the tail hinge-moment derivative due to angle of attack to the tail hinge-moment derivative due to tail deflection) of the tail must be considered. The derivative C_{L_α} represents the sum of the lift force due to angle of attack of the fuselage, the lift force due to angle of attack of the

tail, and the lift force due to tail deflection which is induced by angle of attack. Therefore, C_{L_α} may be expressed as

$$C_{L_\alpha} = \left(C_{L_b}\right)_\alpha + \left(C_{L_t}\right)_\alpha + \frac{d\delta}{d\alpha} C_{L_\delta} \tag{13}$$

Substituting equation (11) into equation (13) results in

$$C_{L_\alpha} = C_{L_\alpha}' + \frac{d\delta}{d\alpha} C_{L_\delta} \tag{14}$$

If the floating characteristics of the tail are assumed to be such that $d\delta/d\alpha$ is a negative quantity, then it can be seen that the value of C_{L_α} is less than the value of C_{L_α}'. With the subject control system the derivative C_{L_α} is equivalent to the derivative C_{L_α} of a configuration having a conventional control system with stick free.

The term C_{L_δ} appearing in equations (3) and (13) is the lift derivative due to tail deflection and may be expressed as the sum of the lift derivatives due to the servoplane, stabilizer, and flap. Thus,

$$C_{L_\delta} = \left(C_{L_c}\right)_\delta + \left(1 - \frac{d\epsilon}{d\delta}\right)\left(C_{L_s}\right)_\delta + rC_{L_{\delta_f}} \tag{15}$$

Substituting equation (12) into equation (15) results in

$$C_{L_\delta} = \left(C_{L_t}\right)_\alpha + rC_{L_{\delta_f}} \tag{16}$$

where $\left(C_{L_t}\right)_\alpha$ is assumed equivalent to $\left(C_{L_t}\right)_\delta$ as previously stated.

The term $C_{L_{\delta_c}}$ appearing in equation (3) is the lift derivative due to servoplane deflection and represents the sum of the lift force produced by deflecting the servoplane and the lift force resulting from servoplane downwash on the stabilizer. Therefore,

$$C_{L_{\delta_c}} = \left(C_{L_c}\right)_{\delta_c} + \frac{d\epsilon}{d\delta_c}\left(C_{L_s}\right)_\delta \tag{17}$$

Reduction of Data

Rocket-model tests.- As previously discussed, the method of conducting the rocket-model tests was to pulse the servoplane in a square-wave manner and to observe the response of the free-floating tail and model. The mass and aerodynamic stability relationship between the complete model and the free-floating tail was such that a complete transient response of the model was not obtained during one servoplane pulse interval; however, a complete transient response of the free-floating tail was obtained. From the tail transient response thus obtained, the frequency of oscillation of the tail was determined, and the tail hinge-moment derivative C_{h_δ} was computed by using the following relationship:

$$C_{h_\delta} = -\frac{4I_{Y_t}\pi^2 f^2}{57.3qS\bar{c}}$$

The above relationship neglects the effect of tail-damping moments because in the present system the damping moments are quite small and do not have an appreciable effect on the C_{h_δ} values computed.

Values of the tail damping derivatives $C_{h_{\dot{\delta}}} + C_{h_{\dot{\alpha}}}$ were determined by fairing a damping envelope about the tail transient oscillations, measuring the time required for the oscillation to damp to one-half amplitude, and substituting the time so measured into the following relationship:

$$C_{h_{\dot{\delta}}} + C_{h_{\dot{\alpha}}} = \frac{4I_{Y_t}V(\log_e 0.5)}{57.3qS\bar{c}^2T_{1/2}}$$

The above relationship is based on the assumption that the free-floating tail has only one degree of freedom which is rotation about its hinge axis. In the present tests the rate of change of angle of attack and angle of pitch of the model is quite small and may be considered negligible when compared with the rate of change of tail deflection.

Servoplane effectiveness in changing the trim deflection of the horizontal tail unit is represented by values of $\Delta\delta/\Delta\delta_c$. Values of $\Delta\delta$ are determined by fairing a mean line through the tail transient oscillations and by cross-plotting the trim tail deflection so determined against α. Then, at constant values of α the change in tail trim deflection due to a change in servoplane deflection can be determined.

Figure 10 shows typical plots of tail deflection against angle of attack. These plots show a hysteresis effect or phase difference between tail deflection and angle of attack. This phase difference arises from the incompatibility of the frequency-response characteristics of the model and the free-floating tail, as well as from the fact that the tail was not dynamically balanced about the model center of gravity; however, it does not cause any serious difficulty in reducing the desired information since a mean line can be faired rather simply through the hysteresis loop.

From plots similar to those shown in figure 10 the slope of δ against α can be measured. The $d\delta/d\alpha$ values so determined represent the floating characteristics of the free-floating tail as angle of attack is changed and, as shown by equation (7) of the preceding section, are proportional to the ratio of C_{h_α} to C_{h_δ}. It should be noted that the term $d\delta/d\alpha$ as considered in this paper does not in any way represent the effectiveness of the tail in changing the angle of attack of the complete model.

After values of $d\delta/d\alpha$ and C_{h_δ} are obtained, values of C_{h_α} may be computed by use of equation (7). By equation (9), values may also be computed for $C_{h_{\delta_f}}$. In the present tests the value of the flap linkage ratio is $r = 1$. Values of the servoplane effectiveness as determined by $\Delta\delta/\Delta\delta_c$ may be considered equivalent to $d\delta/d\delta_c$ if nonlinearities are neglected. In the present tests, the values of $\Delta\delta_c$ are small and, consequently, the effects of nonlinearities would be expected to be small. Therefore, if $\Delta\delta/\Delta\delta_c$ is assumed equivalent to $d\delta/d\delta_c$, by equation (5), values may be computed for $C_{h_{\delta_c}}$. Thus, by either directly or indirectly measuring C_{h_δ}, $d\delta/d\alpha$, and $\Delta\delta/\Delta\delta_c$, the quantities C_{h_α}, $C_{h_{\delta_c}}$, and $C_{h_{\delta_f}}$ may be computed.

The lift derivatives C_{L_α}, C_{L_α}', and C_{L_δ} were determined by measuring the slope of cross plots of the variation of C_L with α or δ. In the Mach number ranges where it was not possible to determine directly values for each of the three lift derivatives, equation (14) was used to compute values for any one of the three derivatives where values for the other two could be measured.

Wind-tunnel tests.- Figure 11 presents the δ against α data obtained from wind-tunnel tests of the original configuration and is similar to the data obtained from tests of the small servoplane. These data were cross-plotted and the slopes of the cross plots were measured to obtain $d\delta/d\delta_c$ data. Data on $d\delta/d\alpha$ were obtained by measuring the slopes of the curves in figure 11.

RESULTS AND DISCUSSION

Servoplane Effectiveness

Wind-tunnel tests.- Figures 12 and 13 present servoplane effectiveness data obtained from the low-speed wind-tunnel tests in the form of the variation of servoplane effectiveness with servoplane deflection and with angle of attack for both the original and small servoplanes. The data for the original configuration show increasing effectiveness at positive angles of attack as the servoplane deflection changes in the positive direction and show increasing effectiveness at positive deflections as angle of attack is increased. At an angle of attack of 0°, servoplane effectiveness is constant at a value of $\frac{\partial \delta}{\partial \delta_c} = 0.22$ over the servoplane-deflection range of these tests. Inspection of the data shown in figure 11 indicates that a primary contributing factor to the nonlinearities in servoplane effectiveness is the change in floating characteristics of the free-floating tail as angle of attack is increased. At any constant servoplane deflection the tendency of the tail to float into the wind decreases as angle of attack increases. Consequently, at high angles of attack, servoplane effectiveness could be expected to increase.

The effectiveness data for the small servoplane show trends somewhat different from those of the original servoplane. At constant angles of attack the effectiveness of the small servoplane increases as the servoplane deflection changes in the negative direction; however, at constant servoplane deflection, the effectiveness again increases with increasing angle of attack. As with the original servoplane, the tendency of the free-floating tail to float into the wind decreases with increasing angle of attack and results in increased servoplane effectiveness at high angles of attack. The angle-of-attack range over which the free-floating tail maintains a comparatively constant floating tendency is greater with the small servoplane than with the original servoplane, and the floating tendency is, of course, greater with the small servoplane since decreasing the servoplane area decreases the aerodynamic balance of the tail. The effectiveness of the small servoplane is only 68 percent of the effectiveness of the original servoplane at an angle of attack of 0° and a servoplane deflection of 0°; however, at an angle of attack of 10° and a deflection of -4° the small servoplane is 89 percent as effective as the original servoplane. Consequently, these data indicate that the servoplane downwash effects are appreciable, particularly at high angles of attack where a decrease in servoplane area to approximately 80 percent of the original does not result in a proportionate decrease in servoplane effectiveness.

Rocket-model tests.- Figure 14 presents servoplane-effectiveness data obtained from the two rocket-model tests. These data are presented in the form of the ratio of change in tail deflection to the incremental change in servoplane deflection against Mach number and show that there are no abrupt changes in effectiveness as Mach number is increased up to $M = 1.2$. At an angle of attack of 0° servoplane effectiveness is practically constant at a value of $\Delta\delta/\Delta\delta_c$ of 0.27 up to $M = 0.95$ but decreases gradually as Mach number is increased from 0.95 to 1.1. At an angle of attack of 5° the effectiveness is greater than at an angle of attack of 0° and increases from $M = 0.95$ to a peak at $M = 1.0$ and then decreases gradually as Mach number increases to 1.15. The loss in effectiveness as Mach number increases does not exceed 27 percent of the subsonic values. These rocket-model data are in good agreement with the wind-tunnel data when the fact that incremental values of servoplane deflection are used to obtain the rocket model data and the fact that the wind-tunnel tests indicate large variations in effectiveness with servoplane deflection are considered. The increased effectiveness at an angle of attack of 5° is also in agreement with wind-tunnel tests for the servoplane-deflection range used on model A ($\delta_c = 1^\circ$ to -2°). The effectiveness data obtained from model B were limited to subsonic speeds and angles of attack between 0° and 5°. The data from model B are in reasonable agreement with model A since the wind-tunnel tests show that at more negative servoplane deflections the differences in effectiveness between angles of attack of 0° and 5° are small, and the servoplane deflection range used on model B was $\delta_c = 0^\circ$ to -3.7°.

Tail-Floating Characteristics

Mach number effect.- Figures 15 and 16 present tail-floating characteristics data in the form of the variation of $d\delta/d\alpha$ with Mach number as obtained from rocket-model tests. Figure 15 shows data at constant angles of attack for one servoplane position on each model, and figure 16 shows data at each servoplane position on both models at two angles of attack. These data show that at constant angles of attack and servoplane deflections the values of $d\delta/d\alpha$ are fairly constant with Mach number at subsonic speeds; however, at $M \approx 0.96$ the values dip sharply to a bucket. As Mach number increases above $M \approx 0.96$, $d\delta/d\alpha$ increases rapidly to a peak at approximately $M = 1.2$ and decreases gradually as Mach number further increases to 1.46 which is the highest Mach number reached in these tests.

These $d\delta/d\alpha$ data are comparable with the conventional control parameter $C_{h_\alpha}/C_{h_\delta}$; however, in the present control system the derivatives C_{h_δ} and C_{h_α} are not directly related to the pilot's stick forces as with a conventional control system but are indicative of the floating

tendency or aerodynamic balance of the free-floating tail about its pivot axis. In this control system the pilot's stick forces arise from the servoplane only and not from the complete horizontal tail. When considered in this manner, the significance of values of $d\delta/d\alpha$ is that low negative values indicate that the tail has only a slight tendency to float into the wind. Consequently, at subsonic speeds where values of $d\delta/d\alpha$ are low, this free-floating tail tends to act as a fixed tail and would be expected to make an appreciable contribution to the static stability and damping of an airplane on which it might be employed. At high Mach numbers where the tail-floating tendency is high, as indicated by large negative values of $d\delta/d\alpha$, the tail contribution to airplane static stability and damping would be decreased. Since the static stability of most airplane configurations tends to increase at high Mach numbers, a decrease in the stability contribution of this type tail would probably be desirable; however, the damping of many airplanes tends to decrease at high Mach numbers and high altitudes (refs. 8 and 9), and a decrease of the tail contribution to airplane damping may be of some significance.

Angle-of-attack effect.- Figures 17 and 18 show the variation of $d\delta/d\alpha$ with angle of attack at constant servoplane deflections and subsonic speeds. The data in figure 17 are a comparison of rocket-model and wind-tunnel results, and the data in figure 18 are wind-tunnel results showing a comparison of the data obtained with the original and small servoplanes and with the servoplane removed. These data show that the negative floating tendency of the tail, as indicated by negative values of $d\delta/d\alpha$, decreases steadily as angle of attack increases. In the rocket-model tests the tail approaches a zero floating tendency above an angle of attack of 10°, whereas in the wind-tunnel tests of the original configuration at $\delta_c = 0^\circ$ the tail has zero floating tendency at an angle of attack of 10° and a positive floating tendency as angle of attack increases above 10°. Other unpublished low-speed wind-tunnel tests show the tail-floating tendency to be zero at an angle of attack of 8° and positive at higher angles of attack. The tail-floating tendency at small negative angles of attack is greater than at positive angles of attack for the 0° servoplane position; however, as angle of attack increases negatively, the tail-floating tendency gradually decreases. The rocket-model data presented in figure 15 also show decreasing values of $d\delta/d\alpha$ with increasing angle of attack, and in figure 15(a), where $\delta_c = 1^\circ$, show that at an angle of attack of -5° the values of $d\delta/d\alpha$ are greater than at positive angles of attack.

The agreement between rocket-model and wind-tunnel data is not particularly good even though similar trends are indicated; however, there are several factors which may have considerable influence on the data. As previously described, the wind-tunnel model used had a shorter body than the rocket model; and at high angles of attack the nose of the model was very near the tunnel ceiling, whereas at large negative angles of attack the tail was near the tunnel ceiling. No attempt has been made

to apply any corrections to the wind-tunnel data since these tests were only preliminary to the rocket-model tests. As previously discussed and illustrated in figure 10, the plots of δ against α obtained from the rocket-model tests show a hysteresis effect which must be faired out in order to obtain values of $d\delta/d\alpha$. Such fairing is a logical source of small discrepancies in the data obtained. The large difference in results obtained at high angles of attack is probably primarily due to tunnel-wall and support-strut interference.

Servoplane effect.- The data of figure 18 show that reducing the servoplane area to 80 percent of the area of the original servoplane results in a large increase in both the tail-floating tendency and the angle-of-attack range over which the tail-floating tendency is negative and also tends to make the floating tendency more nearly constant with angle of attack. At high angles of attack, however, the tail still becomes overbalanced. With the servoplane removed from the tail, the floating tendency is increased greatly and tends to increase rather than decrease at high angles of attack. A comparison of these data leads to the conclusion that servoplane downwash effects on the floating characteristics of the free-floating tail are nonlinear with angle of attack, being particularly large at high angles of attack, and are overbalancing.

Servoplane deflection has a large effect on the floating tendency of the free-floating tail. Figures 18 and 19 show this effect. Figure 19 is a plot of the variation of $d\delta/d\alpha$ with servoplane deflection at constant angles of attack for both servoplane configurations as obtained from the wind-tunnel tests. These data show for the original configuration that at positive angles of attack the tail-floating tendency increases and at negative angles of attack decreases as servoplane deflection is changed in the negative direction. At an angle of attack of 0° there is little effect of servoplane deflection on the tail-floating characteristics through the servoplane-deflection range of these tests. For the small servoplane, however, there is little effect of servoplane deflection at any angle of attack within the range of these tests. As indicated by a comparison of the data in figures 16, 18, and 19(a) the agreement between wind-tunnel and rocket-model data is good. In figure 16(a) where $\alpha = 0^\circ$ servoplane deflection again has little effect on the tail-floating tendency, and in figure 16(b) where $\alpha = 5^\circ$ the tail-floating tendency increases as servoplane deflection increases negatively. Also the rocket-model data presented in figure 17, like the wind-tunnel data in figure 19, show that changing servoplane deflection in the negative direction increases the tail-floating tendency at positive angles of attack and decreases it at negative angles of attack. In a practical application of this control system to an airplane, negative servoplane deflections would be required to produce positive angles of attack. Therefore, the decrease in tail-floating tendency with increasing angle of attack would be partially compensated for by the increase in tail-floating tendency at negative servoplane deflections.

Hinge Moments

In this discussion the hinge-moment derivatives considered are those of the tail unit or its components about the tail pivot axis and have no significance as to the pilot's stick forces. All the data presented represent the hinge moments against which the servoplane must work in changing the free-floating-tail trim deflection or lift force. The servoplane hinge moments or pilot's stick forces have not been considered.

C_{h_δ}.- Figure 20 is a plot of the hinge-moment derivative C_{h_δ} against Mach number at each of the two servoplane positions employed on the two rocket models. As previously stated, these data are computed from the measured period of the transient oscillations in tail deflection following a change in servoplane deflection. Although the data from the two models are not in exact agreement, the general trends shown are similar. In each test the data obtained at positive servoplane deflections shows higher values of C_{h_δ} than are shown at negative servoplane deflections. During the time that these data are obtained, the range of δ and α is variable. Generally, the data at negative servoplane deflections correspond to higher angles of attack than those at positive servoplane deflections, and the angle of attack increases as Mach number increases. Insufficient data are available to plot curves at constant angles of attack or tail deflection; therefore, the individual effects of servoplane deflection and angle of attack on the value of C_{h_δ} cannot be established definitely. However, the decrease in values of C_{h_δ} at negative servoplane deflections and high angles of attack would be expected to result in increased servoplane effectiveness under such conditions, and figure 14 indicates that this is true. In figure 14 the servoplane effectiveness for model A is shown to be greater at $\alpha = 5^\circ$ than at $\alpha = 0^\circ$.

The variation of C_{h_δ} with Mach number is not large, but C_{h_δ} tends to increase as Mach number increases. However, above $M = 0.95$ it is irregular, whereas below this speed it is comparatively smooth. Unpublished low-speed wind-tunnel tests show that $C_{h_\delta} = -0.0093$, which is in good agreement with these data. Since there are no large or abrupt changes in C_{h_δ} with Mach number, servoplane effectiveness would be expected to remain reasonably constant with Mach number, and figure 14 indicates that such is the case, the irregularities above $M = 0.95$ corresponding to the irregularities in C_{h_δ} above $M = 0.95$. Since the derivative C_{h_δ} is complex, as pointed out in the section on "Method of Analysis," the irregularities in C_{h_δ} above $M = 0.95$ may be considered as the result of changes in the quantities C_{h_α} and $C_{h_{\delta_f}}$ which make up C_{h_δ}.

C_{h_α}.- As described previously in this paper, values may be computed for the partial hinge-moment derivative C_{h_α} by combining the C_{h_δ} and $d\delta/d\alpha$ data obtained. Figure 21 presents this information plotted against Mach number. The curves for δ_c values of 0°, -2°, and -3.73° are derived from the data of figures 16(b) and 20 at $\alpha = 5^\circ$ and the curve for $\delta_c = 1^\circ$ from the data of figures 16(a) and 20 at $\alpha = 0^\circ$. In each case the angle of attack selected for computing these data represents the angle-of-attack range in which most of the data were obtained. With the exception of the data at $\delta_c = -3.73^\circ$, the C_{h_α} data thus computed show good agreement for the servoplane positions used and also show that the value of C_{h_α} remains nearly constant with Mach number at subsonic speeds up to $M \approx 0.95$. At $M \approx 0.95$, the values dip sharply to a bucket and increase rapidly to $M = 1.0$. Above $M = 1.0$, C_{h_α} continues to increase to $M = 1.15$ which is the highest speed where C_{h_δ} data were obtained. These data seem to indicate that at small servoplane deflections there is little effect of either servoplane position or angle of attack on the values of C_{h_α}, particularly at subsonic speeds. The low value of C_{h_α} at subsonic speeds indicates that the center of pressure of the tail unit is only slightly back of the tail pivot axis, and, as Mach number increases, the center of pressure first moves forward almost to the pivot axis at $M \approx 0.95$ and thereafter moves rearward fairly rapidly as Mach number increases.

$C_{h_{\delta_f}}$.- The data for $C_{h_{\delta_f}}$ as obtained from the difference in C_{h_δ} and C_{h_α} are also presented in figure 21 along with the C_{h_δ} data of figure 20 which has been repeated for purposes of comparison. These data show that the values of $C_{h_{\delta_f}}$ increase gradually with Mach number up to $M \approx 0.95$ and then decrease sharply as Mach number increases to $M = 1.1$. Above $M = 1.1$ the values tend to level out. As pointed out previously, this derivative represents the sum of the flap hinge moments about the flap hinge line and the moment about the pivot axis produced by the flap lift forces. Generally, at transonic speeds the lift effectiveness of a plain flap decreases whereas the hinge moments increase sharply (refs. 10 and 11). Thus, in the present case, the data indicate that the change in hinge moment resulting from a loss in flap lift effectiveness is greater than the change resulting from an increase in flap hinge moments up to $M = 1.1$. Above $M = 1.1$ up to the limit of these data, the two effects apparently equalize.

The differences in $C_{h_{\delta_f}}$ at the different values of δ_c are comparatively large and are greater at subsonic speeds than at supersonic speeds. These differences may be attributed to differences in α, δ,

or δ_c; however, they apparently are primarily due to δ_c and δ, the differences in C_{h_α} being small.

In comparing these C_{h_δ}, C_{h_α}, and $C_{h_{\delta_f}}$ data it can be seen that the geometric and aerodynamic arrangement of this free-floating tail unit is such that the increase in C_{h_α} at transonic speeds is counteracted by a decrease in $C_{h_{\delta_f}}$ which results in a practically constant value of C_{h_δ} through the transonic-speed range. Thus, a satisfactory balance is achieved which allows the use of a relatively simple aerodynamic servo to change the tail trim. The applicability of this control system to an airplane configuration is, of course, dependent on many factors other than its hinge-moment characteristics, and the system readily lends itself to many modifications for the purpose of obtaining desired characteristics.

$C_{h_{\delta_c}}$.- As previously shown, values may be computed for the partial hinge-moment derivative $C_{h_{\delta_c}}$ by combining the C_{h_δ} data of figure 20 and the $\Delta\delta/\Delta\delta_c$ data of figure 14. The values of $C_{h_{\delta_c}}$ so determined are presented in figure 21 and represent the tail-balancing moments due to the servoplane.

These data show that the balancing action of the servoplane is reasonably constant with Mach number. The slight peak at $M = 1$ corresponds to the expected peak in the lift-curve slope for such a lifting surface. Unpublished low-speed wind-tunnel tests show $C_{h_{\delta_c}} = 0.0024$ which is in good agreement with these data.

Tail Damping

The damping characteristics of the free-floating horizontal tail about its pivot axis are presented in figure 22 as a plot against Mach number of values of $C_{h_{\dot{\delta}}} + C_{h_{\dot{\alpha}}}$ which were determined from the two rocket-model tests. These data show that the tail damping derivative remains practically constant over the Mach number range of the tests except in the Mach number range between 0.95 and 1.05. In this range there is first a rapid loss in damping, followed by a rapid recovery. At $M = 0.98$, the tail is dynamically unstable. Figure 23 is a reproduction of a section of the telemeter record obtained from model A and shows the character of the tail oscillations in the unstable range.

In accordance with data presented in reference 8, this loss of damping would not be expected; however, the influence of the vertical tail and

the intersection of the vertical and horizontal tails is not known. Unpublished wind-tunnel tests made in the Langley 8-foot transonic wind tunnel of tail configurations similar to the one being investigated here agree well with these damping data. In these wind tunnel tests, the loss of tail damping occurred at a slightly higher Mach number range. Also, the wind-tunnel tests indicated that the influence of the vertical tail was primarily responsible for the loss of tail damping and resultant large oscillations. In applying the tail to an airplane, this instability would not be expected to be a matter of serious consequence, since a mechanical damper could easily be included in the design.

The agreement between data obtained at the different servoplane deflections is good, and the small differences shown may be attributed to differences in angle of attack and tail deflection as well as servoplane position.

In reducing these damping data from the present tests, it was noted that there was a reasonably consistent variation of damping with the amplitude of the tail oscillation regardless of the tail trim deflection. At amplitudes greater than $\delta = 0.6^\circ$, there was no appreciable variation of damping with amplitude; however, at amplitudes less than 0.6°, damping increased rapidly as amplitude decreased until at an amplitude of 0.4° the values of $C_{h_{\dot{\delta}}} + C_{h_{\dot{\alpha}}}$ are about twice the values at higher amplitude. As the oscillation amplitude decreases further to 0.2° the damping decreased to values of the same order as at the high amplitudes. All the data shown in figure 22 were obtained from tail oscillations having amplitudes greater than $\delta = 0.6^\circ$.

Lift

Data for three different lift derivatives have been obtained from these rocket-model tests. Two of these derivatives, C_{L_α} and $C_{L_{\alpha'}}$, refer to the complete rocket-model configuration, whereas the third C_{L_δ} represents the lift or maneuvering effectiveness of the horizontal tail and is of primary importance in this paper. As previously mentioned, in the Mach number ranges where these three derivatives could not be individually determined, values have been computed for any one of them where values of the other two were measured.

Tail lift.- Figure 24 presents the tail lift effectiveness data obtained from rocket model B and shows the variation of C_{L_δ} with Mach number. The dashed portion of this curve represents values computed from measured values of related quantities. These data show that C_{L_δ} is nearly constant with Mach number up to $M = 1.15$ at which speed it

starts to decrease and tends to level out again as Mach number reaches 1.4. Tail lift effectiveness at $M = 1.4$ is still 70 percent of subsonic effectiveness.

The comparative constancy of the lift effectiveness through the transonic speed range together with the high C_{L_δ} values obtained indicate that this control system might be very satisfactory from a maneuvering point of view when applied to a transonic airplane configuration. The unconventionally high values of C_{L_δ} shown are commensurate with an all-movable tail having a linked unbalancing flap.

The fact that the value of C_{L_δ} remains nearly constant up to $M = 1.15$ can be attributed to two causes. As previously shown C_{L_δ} represents the sum of the lift forces due to tail deflection and to flap deflection. Hinge-moment data presented in figure 21 indicated that flap lift effectiveness decreased rapidly above $M = 0.95$; however, model lift data obtained with the tail fixed and presented later in this paper show that the tail lift increases above $M = 0.95$. This gain in tail lift compensates for the loss in flap lift and results in a nearly constant C_{L_δ} up to $M = 1.15$. Above $M = 1.15$ tail lift decreases slightly; thus, C_{L_δ} also decreases.

C_{L_δ} data were not obtained from model A, and it was not possible to determine values for the servoplane lift derivative $C_{L_{\delta_c}}$ from either model.

Model lift.- Figure 25 shows the variation of complete-model lift derivatives C_{L_α} and C_{L_α}' with Mach number. Again the dashed portion of the C_{L_α}' curve represents computed values. These C_{L_α} data are the model lift derivative with the tail free and represent the effectiveness of the tail in adding static stability to an airplane configuration on which it might be employed. The data show that C_{L_α} is constant with Mach number at subsonic speeds, rises to an abrupt peak at $M \approx 0.96$, and thereafter decreases gradually as Mach number increases to $M = 1.2$. Above $M = 1.2$ the values tend to level out at about 70 percent of the subsonic values. These data are in good agreement with the tail-floating characteristics data since at supersonic speeds where the tail-floating tendency is high its contribution to total lift is decreased. The fact that there is only a 30-percent reduction in tail lift effectiveness through the Mach number range shows that the linked flap serves its purpose well in making the tail provide a stability contribution to an airplane.

The higher values of C_{L_α} obtained from model B as compared to those obtained from model A are a result of the fact that model B was in a higher angle-of-attack range throughout its flight than was model A. The tail-floating characteristics data presented previously show that the tail-floating tendency decreases as angle of attack increases; therefore, the tail lift contribution would be greater at high angles of attack than at low angles of attack. Insufficient lift data were obtained to allow presenting C_{L_α} data at constant angles of attack.

The C_{L_α}' data shown are the model lift derivative with the tail fixed and, since fuselage lift is only a small percentage of the total, represent the lift characteristics of the tail when the flap is considered fixed. These data were obtained during portions of the flight of model B when the tail was against one of its deflection stops and was effectively fixed. Insufficient data were obtained from model A to plot similar data. These data show that the tail-fixed lift increases gradually with Mach number above $M = 1.0$ to a peak at $M = 1.2$ and thereafter decreases until at $M = 1.4$ the values are nearly the same as at subsonic speeds. The increase in lift effectiveness above $M = 1.0$ counteracts the loss in flap lift effectiveness previously shown and results in the sustained maneuvering and airplane stability effectiveness of the tail through the transonic speed range. Also, this increase in lift indicates that the increase in C_{h_α} previously shown is due partially to the lift increase as well as to rearward movement of the tail center of pressure.

These C_{L_α}' data compare favorably with C_{L_α} data presented in references 10 and 11. The fact that the peak value of C_{L_α}' occurs at a somewhat higher Mach number than would be expected is due primarily to the increase in C_{L_α} with angle of attack shown in references 10 and 11 as well as by the C_{L_α} data previously presented. In the present tests, the angles of attack are greater at high Mach numbers than at low Mach numbers.

Figure 26 presents the complete-model trim lift-coefficient data obtained at one servoplane position on each rocket model and shows the variation of trim C_L with Mach number at constant angles of attack in the ranges where the tail is free. These data show a sharp negative trim change in the Mach number range between 0.95 and 1.0 which increases in severity as angle of attack increases. At higher Mach numbers there is a positive trim change which continues up to the highest Mach number where data were obtained. The relationship of these curves shows that the lift-curve slope decreases at Mach numbers above 1.0. From the data obtained in these tests it is not possible to determine definitely the

cause of these trim changes; however, tail trim data to be presented later do give some indication of the effects of tail-trim changes.

Tail Trim Characteristics

The free-floating-tail trim characteristics are shown in figures 27 to 29. Figure 27 shows the variation with Mach number of the tail trim deflection at constant angles of attack for one servoplane position on each model, and figure 28 shows this same variation at two angles of attack for each servoplane position on both models. These data show that below $M \approx 0.95$ there is no appreciable change in tail trim deflection with Mach number; however, above $M \approx 0.95$, there is a gradual trim change in the positive direction at $\alpha = 0^\circ$. At $\alpha = 5^\circ$ there is first a negative trim change followed by a positive change as Mach number increases above 0.95, and at $\alpha = 10^\circ$ the changes are similar to the changes at $\alpha = 5^\circ$. In the subsonic speed range the close relative proximity of the trim curves at different angles of attack corresponds to the low tail-floating tendency or low values of $d\delta/d\alpha$ shown in figure 15, and above $M \approx 0.95$ the relative spreading apart of these curves corresponds to the rapidly increasing tail-floating tendency as Mach number increases. Consequently, the basic tail trim change is that shown for $\alpha = 0^\circ$ which is a gradual positive change as Mach number increases above $M \approx 0.95$, and the fact that at positive angles of attack the trim change is first in the negative direction is due to the spreading effect of the rapidly increasing tail-floating tendency.

The data of figure 28 show that there is no appreciable effect of servoplane position on the variation of tail trim with Mach number. The absolute trim position of the tail on one model, however, cannot be compared with the absolute trim position on the other model because of inherent small inaccuracies in absolute values of tail deflection and because of the body boattail fairing on model B. With the possible exception of some slight difference in absolute tail deflection, there is no indication in these data that the body boattail fairing has any appreciable effect on the trim characteristics of this free-floating tail. Also these data in conjunction with data previously presented indicate that the tail trim change as Mach number increases cannot be attributed to any effect of the servoplane on the stabilizer. The most likely explanation of the cause of this tail trim change lies in the interference effects of the vertical tail and between the horizontal and vertical tails at their intersection. Figure 2(c) shows a cross-sectional view of this intersection and reveals the possibility of high positive pressures at the fin leading edge affecting the horizontal-tail area within the tail boom at the juncture. Such an occurrence would be expected to cause a positive hinge moment on the tail and thus produce a positive trim change. Unpublished wind-tunnel tests made in the Langley 8-foot transonic wind tunnel show that the interference effects of the vertical tail and its associated shock patterns are primarily responsible for the tail trim change.

Utilizing equation (4) and hinge-moment data presented in figure 21, together with tail trim data, values have been computed for C_{h_o}. The C_{h_o} values so determined are presented in figure 29 and generally show that the basic tail hinge moment increases positively with Mach number above 0.95 in a manner similar to the tail trim deflection. These data then indicate that the tail trim change is primarily the result of a change in the tail trim hinge moment and that the tail lift is not appreciably affected. This conclusion is borne out by a comparison of the model trim lift coefficients presented in figure 26 with the tail trim deflections shown in figure 27. The variation of model trim lift with Mach number is essentially the same as the variation of tail trim deflection except that the model trim lift seems to decrease slightly between $M = 0.95$ and 1.0 as evidenced at $\alpha = 0^o$.

CONCLUSIONS

Low-speed wind-tunnel tests and rocket-model tests from $M = 0.6$ to $M = 1.46$ of a canard-balanced free-floating all-movable triangular horizontal tail mounted on the tip of a swept vertical tail and having a linked trailing-edge flap indicated the following conclusions:

1. Wind-tunnel tests of both the original and a smaller canard type servoplane show that servoplane downwash has an appreciable overbalancing effect on the floating characteristics of the free-floating tail particularly at high angles of attack.

2. There are no large or abrupt changes in servoplane effectiveness with Mach number up to $M = 1.15$ and agreement between wind-tunnel and rocket-model tests is good.

3. The tendency of the free-floating tail to float into the wind is quite low at subsonic speeds but increases rapidly in the transonic range; thus, the stability and damping contribution that the tail might make to an airplane configuration is decreased. The tail-floating tendency decreases with increasing angle of attack but is partially compensated for by an increased floating tendency at negative servoplane deflections.

4. In the transonic speed range, the hinge-moment derivative due to angle of attack C_{h_α} increases rapidly, but the increase is compensated for by a reduction in the hinge-moment derivative due to flap deflection $C_{h_{\delta_f}}$ which results in an irregular but comparatively steady value of the hinge moment dervative due to tail deflection C_{h_δ} up to the highest

speed reached in these tests. Thus, a satisfactory balance is achieved which allows the use of an aerodynamic servo to change the tail trim.

5. The damping characteristics of the free-floating tail are acceptable in that the sum of the damping derivatives is nearly constant with Mach number except at Mach number 0.98. At Mach number 0.98, the tail is dynamically unstable. A mechanical damper can easily be included in the design.

6. The constancy of the all-movable tail lift effectiveness through the transonic speed range together with the high values of lift due to tail deflection C_{L_δ} obtained indicate that this control might be very satisfactory from a maneuvering point of view when applied to a transonic airplane configuration.

7. The lift characteristics of the complete model indicate that the tail-linked flap serves its purpose well in making the tail provide a stability contribution to the complete configuration throughout the speed range.

8. As Mach number increases above Mach number 0.95 there is a steadily increasing positive trim change in the hinge moment of the free-floating tail which is not appreciably affected by elimination of the body boattail and which is not accompanied by a corresponding change in the tail trim lift. Interference effects of the vertical tail and the juncture of the horizontal and vertical tails are probably the cause of this hinge-moment trim change.

Langley Aeronautical Laboratory,
National Advisory Committee for Aeronautics,
Langley Field, Va., September 28, 1953.

REFERENCES

1. Harmon, Sidney M.: Comparison of Fixed-Stabilizer, Adjustable-Stabilizer, and All-Movable Horizontal Tails. NACA WR L-195, 1945. (Formerly NACA ACR L5H04.)

2. Jones, Robert T., and Kleckner, Harold F.: Theory and Preliminary Flight Tests of an All-Movable Vertical Tail Surface. NACA WR L-496, 1943. (Formerly NACA ARR, Jan. 1943.)

3. Kleckner, Harold F.: Preliminary Flight Research on an All-Movable Horizontal Tail as a Longitudinal Control for Flight at High Mach Numbers. NACA WR L-89, 1945. (Formerly NACA ARR L5C08.)

4. Kleckner, Harold F.: Flight Tests of an All-Movable Horizontal Tail With Geared Unbalancing Tabs on the Curtiss XP-42 Airplane. NACA TN 1139, 1946.

5. Mungall, Robert G.: Flight Investigation of a Combined Geared Unbalancing-Tab and Servotab Control System As Used With an All-Movable Horizontal Tail. NACA TN 1763, 1948.

6. Gillis, Clarence L., and Vitale, A. James: Wing-On and Wing-Off Longitudinal Characteristics of an Airplane Configuration Having a Thin Unswept Tapered Wing of Aspect Ratio 3, As Obtained From Rocket-Propelled Models at Mach Numbers From 0.8 to 1.4. NACA RM L50K16, 1951.

7. Greenberg, Harry, and Sternfield, Leonard: A Theoretical Investigation of Longitudinal Stability of Airplanes With Free Controls Including Effect of Friction in Control System. NACA Rep. 791, 1944. (Supersedes NACA WR L-430.)

8. Gillis, Clarence L., and Chapman, Rowe, Jr.: Summary of Pitch-Damping Derivatives of Complete Airplane and Missile Configurations as Measured in Flight at Transonic and Supersonic Speeds. NACA RM L52K20, 1953.

9. D'Aiutolo, Charles T., and Parker, Robert N.: Preliminary Investigation of the Low-Amplitude Damping in Pitch of Tailless Delta- and Swept-Wing Configurations at Mach Numbers From 0.7 to 1.35. NACA RM L52G09, 1952.

10. Rathert, George A., Jr., Rolls, L. Stewart, and Hanson, Carl M.: The Transonic Characteristics of a Low-Aspect-Ratio Triangular Wing With a Constant-Chord Flap As Determined by Wing-Flow Tests, Including Correlation With Large-Scale Tests. NACA RM A50E10, 1950.

11. Mitcham, Grady L., Crabill, Norman L., and Stephens, Joseph E.: Flight Determination of the Drag and Longitudinal Stability and Control Characteristics of a Rocket-Powered Model of a 60° Delta-Wing Airplane From Mach Numbers of 0.75 to 1.70. NACA RM L51I04, 1951.

TABLE I

GEOMETRIC CHARACTERISTICS OF HORIZONTAL

AND VERTICAL TAILS

Horizontal tail:

Stabilizer:

Delta surface, leading-edge sweepback, deg	63.4
Aspect ratio	2.0
Area, sq ft	1.47
Mean aerodynamic chord, ft	1.14
Airfoil section	GAEC-004 (similar to NACA 0004)
Pivot-axis location, percent mean aerodynamic chord	29
Flap linkage ratio	1:1

Servoplane:

Delta surface, leading-edge sweepback, deg	63.4
Aspect ratio	2.0
Area, sq ft	0.122
Mean aerodynamic chord, ft	0.329
Airfoil section	GAEC-006 (similar to NACA 0006)
Hinge-axis location, percent mean aerodynamic chord	47

Vertical tail (exposed):

Aspect ratio	0.674
Taper ratio	0.444
Area, sq ft	1.91
Span, ft	1.137
Mean aerodynamic chord, ft	1.77
Sweepback of 0.25-chord line	54°26'
Airfoil section (parallel to free stream)	NACA 64A008

TABLE II

MASS CHARACTERISTICS OF ROCKET MODELS

	Model A	Model B
Takeoff weight, lb	199.5	196.5
Burnout weight, lb	173.0	170.0
Takeoff mass, slugs	6.20	6.11
Burnout mass, slugs	5.37	5.28
Takeoff center-of-gravity location (forward of tail pivot axis), ft	2.25	2.01
Burnout center-of-gravity location (forward of tail pivot axis), ft	2.34	2.06
I_Y (burnout), slug-ft^2	28.0	27.5
I_{Y_t}, slug-ft^2	0.143	0.149

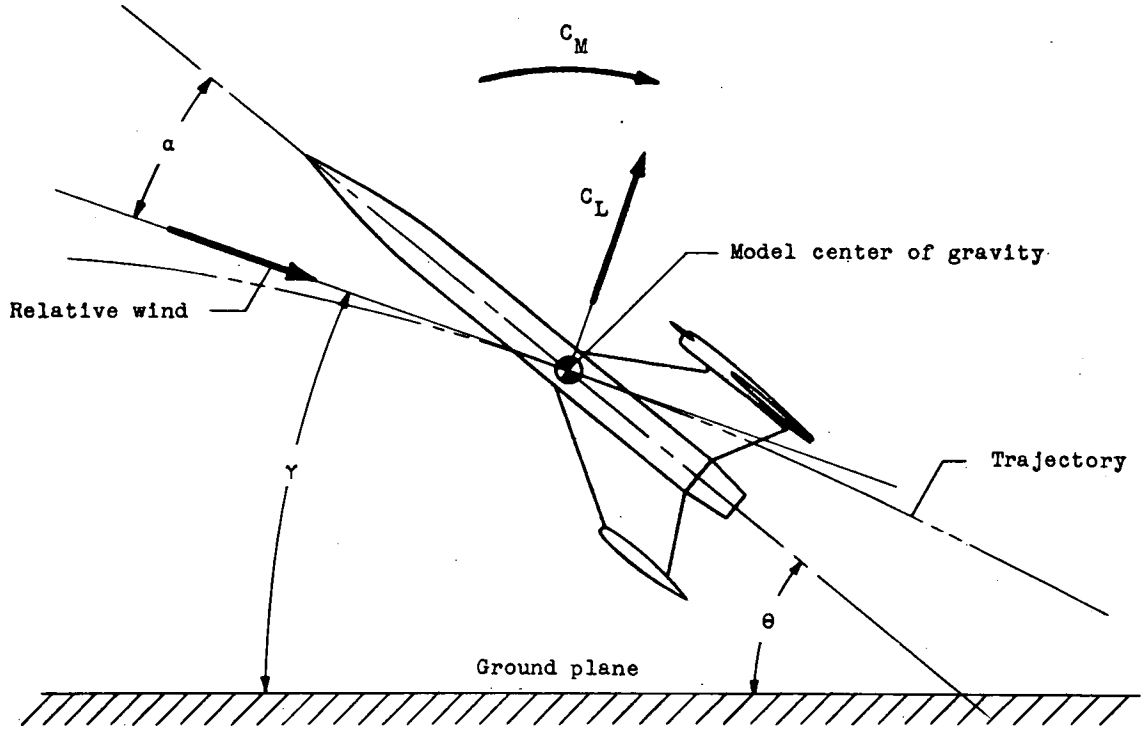

(a) Complete model.

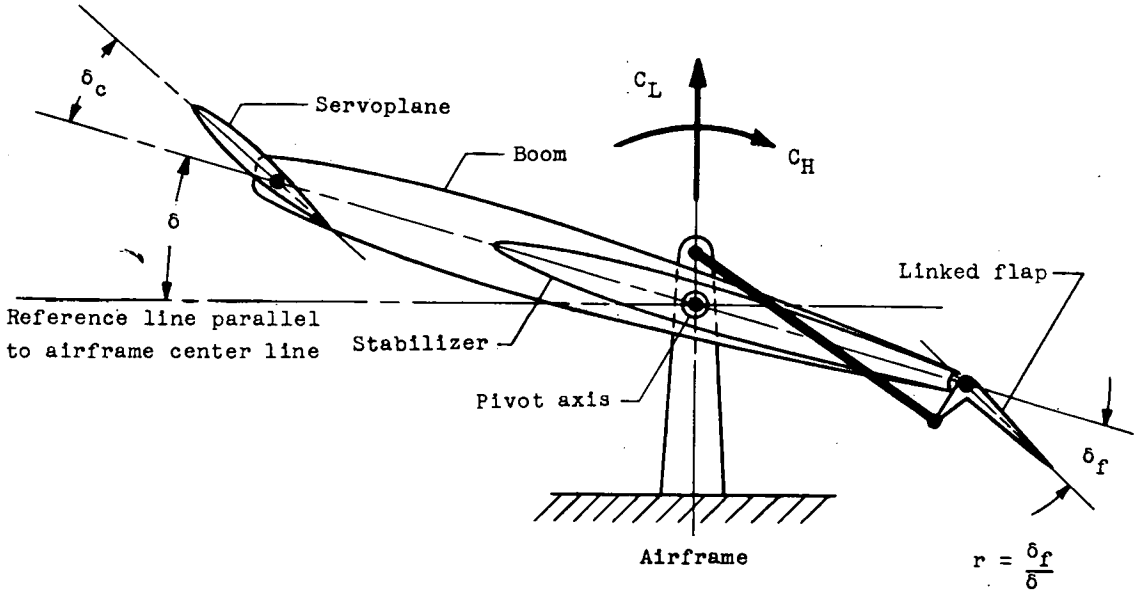

(b) Horizontal tail.

Figure 1.- Sign conventions used for canard-balanced all-movable horizontal tail. All angles, deflections, forces, and moments are shown in positive sense.

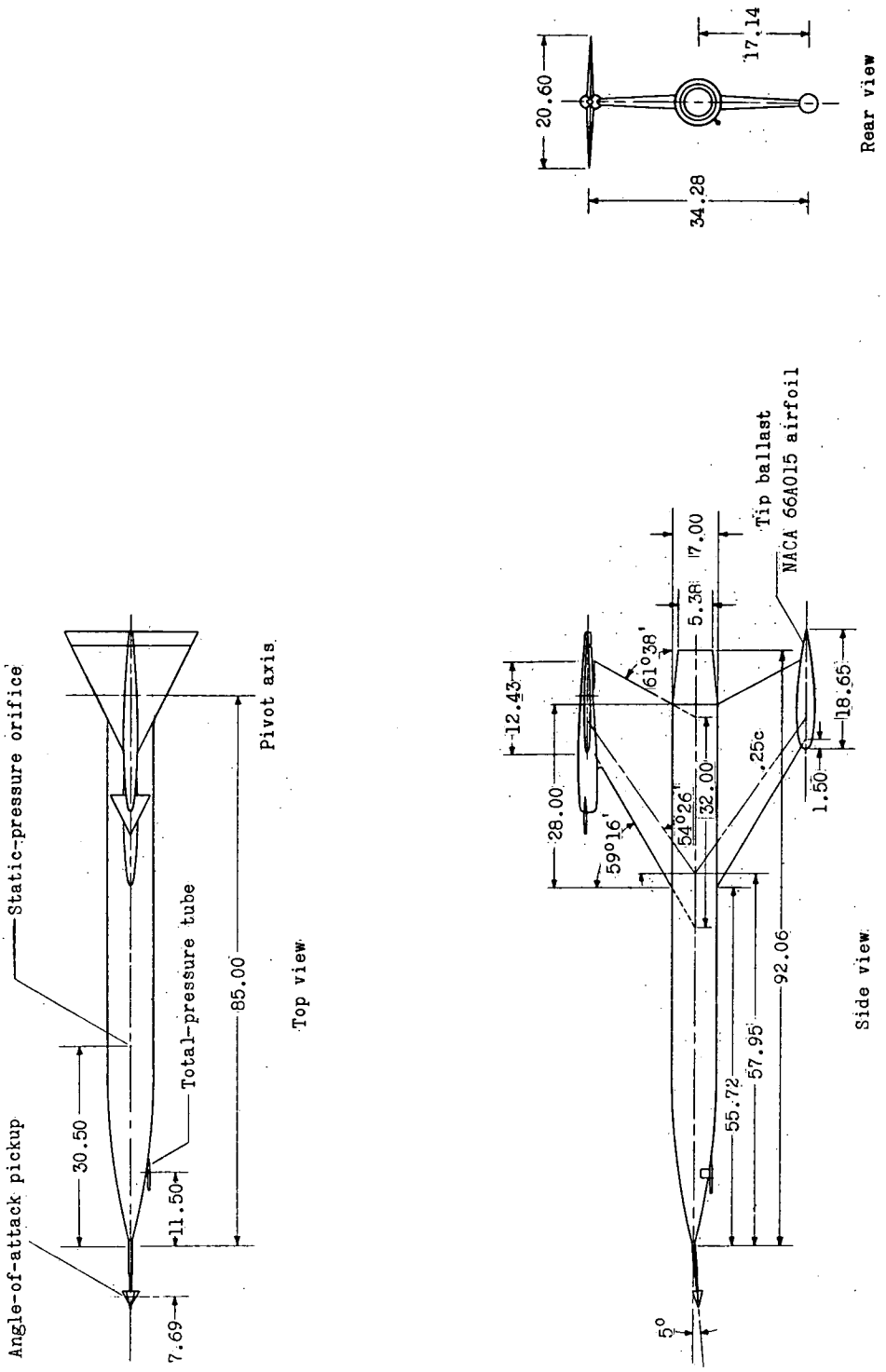

(a) Complete model.

Figure 2.- General arrangement of rocket models. All dimensions are in inches.

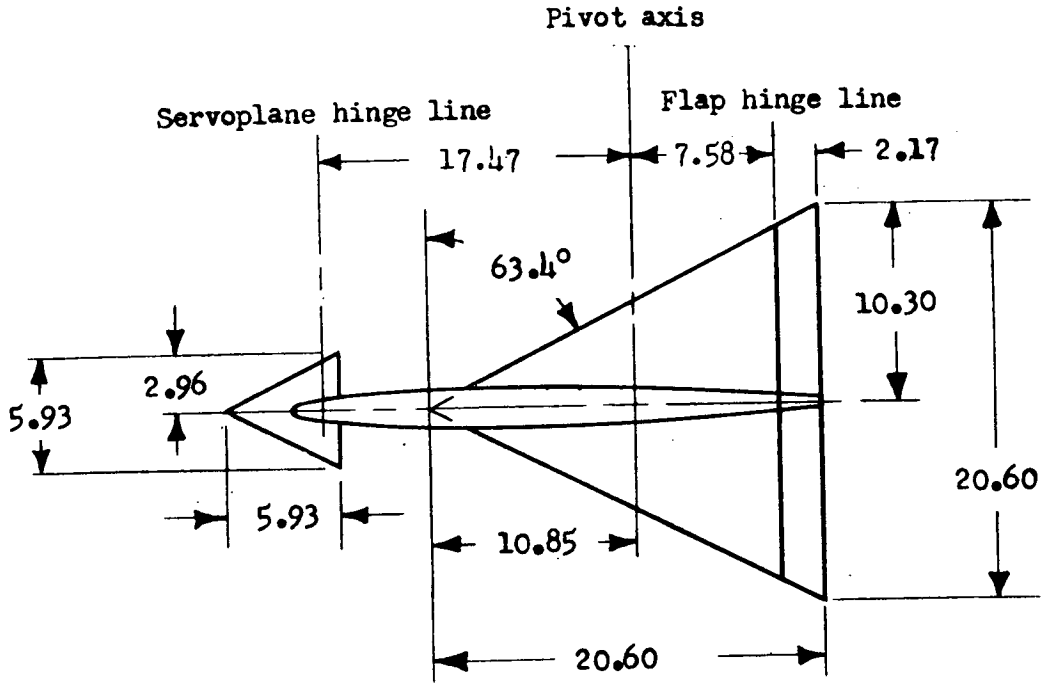

Top view

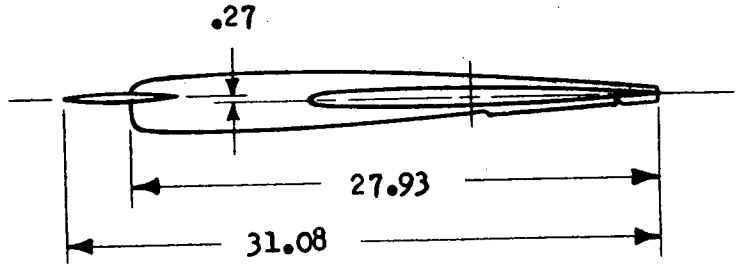

Side view

(b) Horizontal tail.

Figure 2.- Continued.

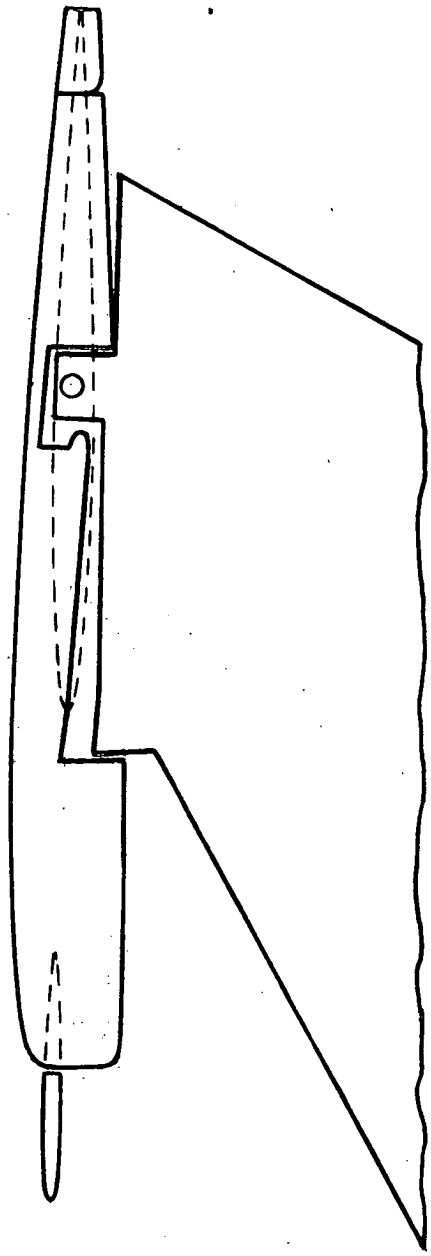

(c) Section view showing intersection of horizontal and vertical tails in plane of symmetry.

Figure 2.- Continued.

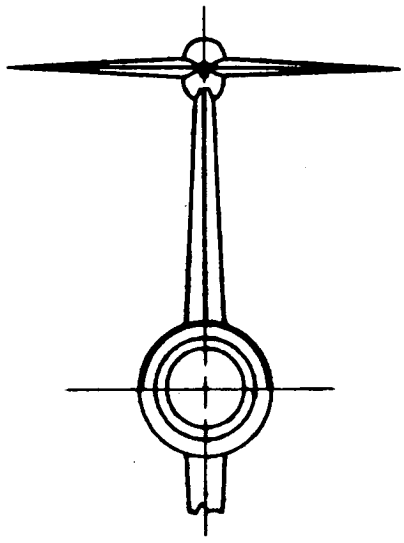

End view

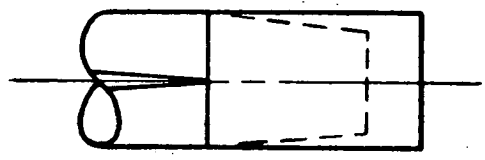

View A-A

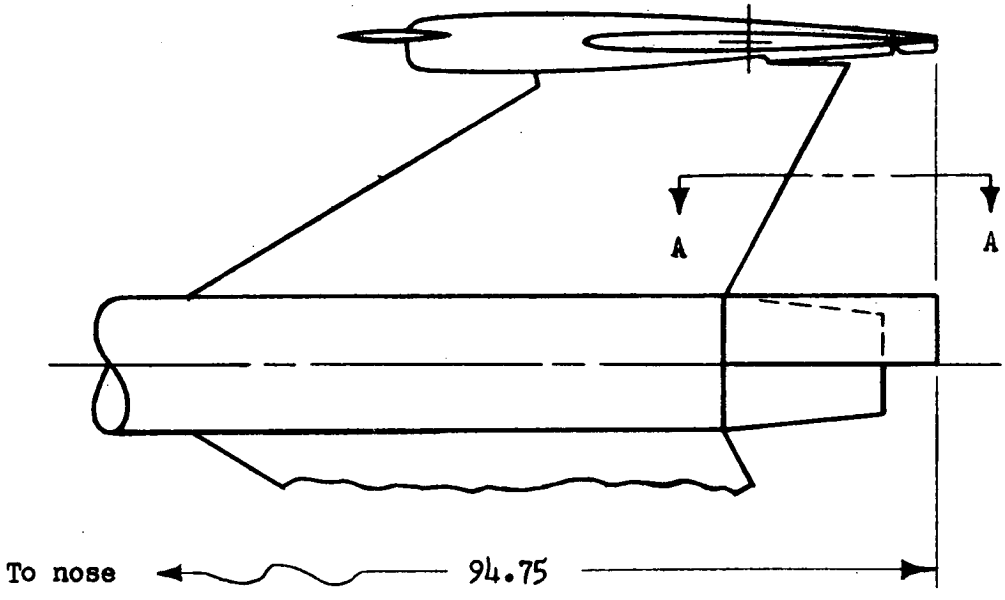

Side view

(d) Boattail fairing.

Figure 2.- Concluded.

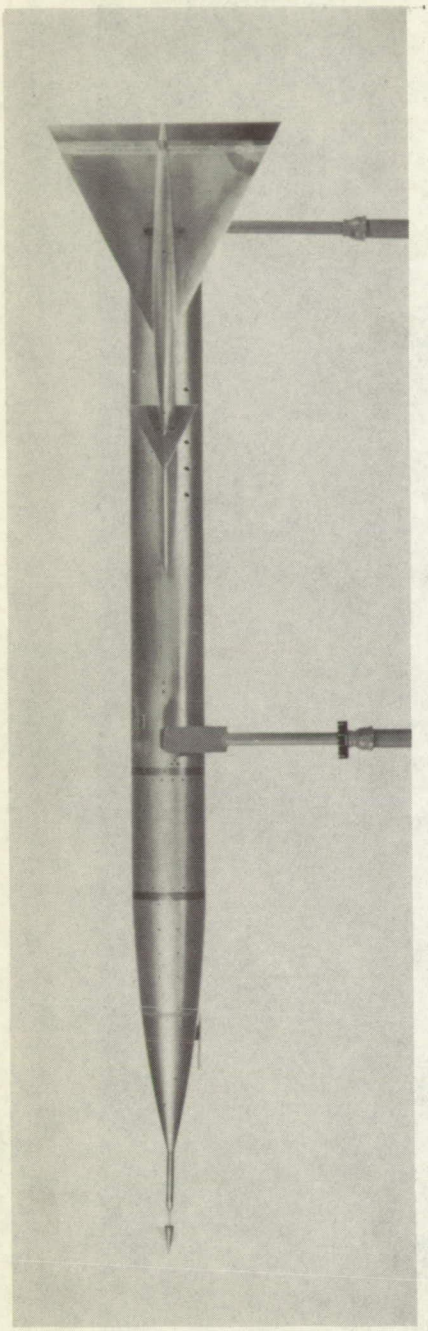

L-71240.1

(a) Top view.

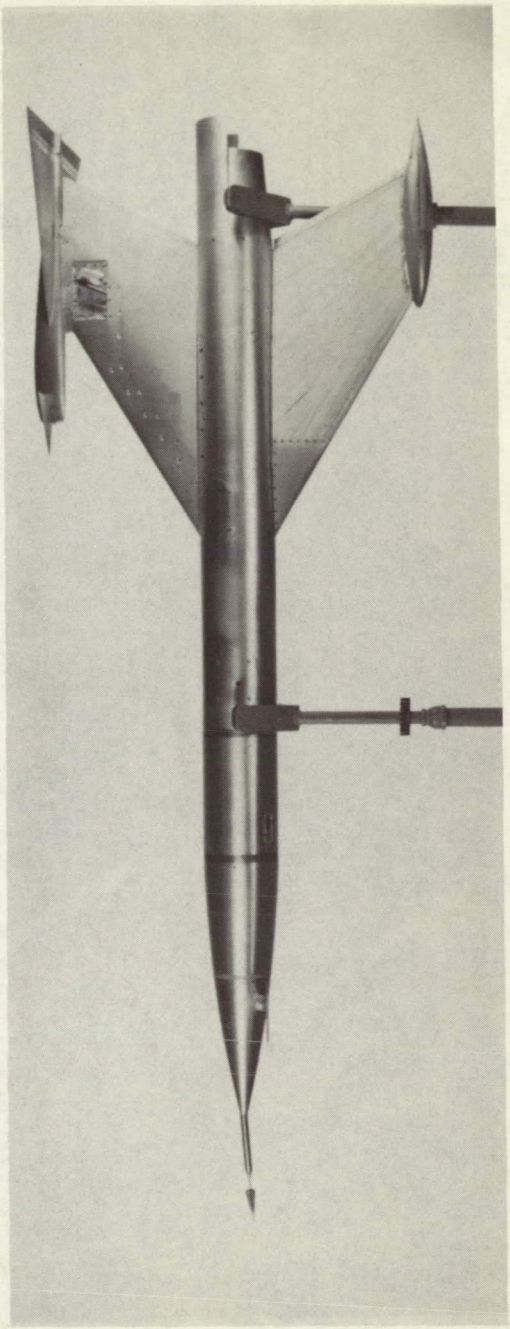

L-71242.1

(b) Side view.

Figure 3.- Complete model tested.

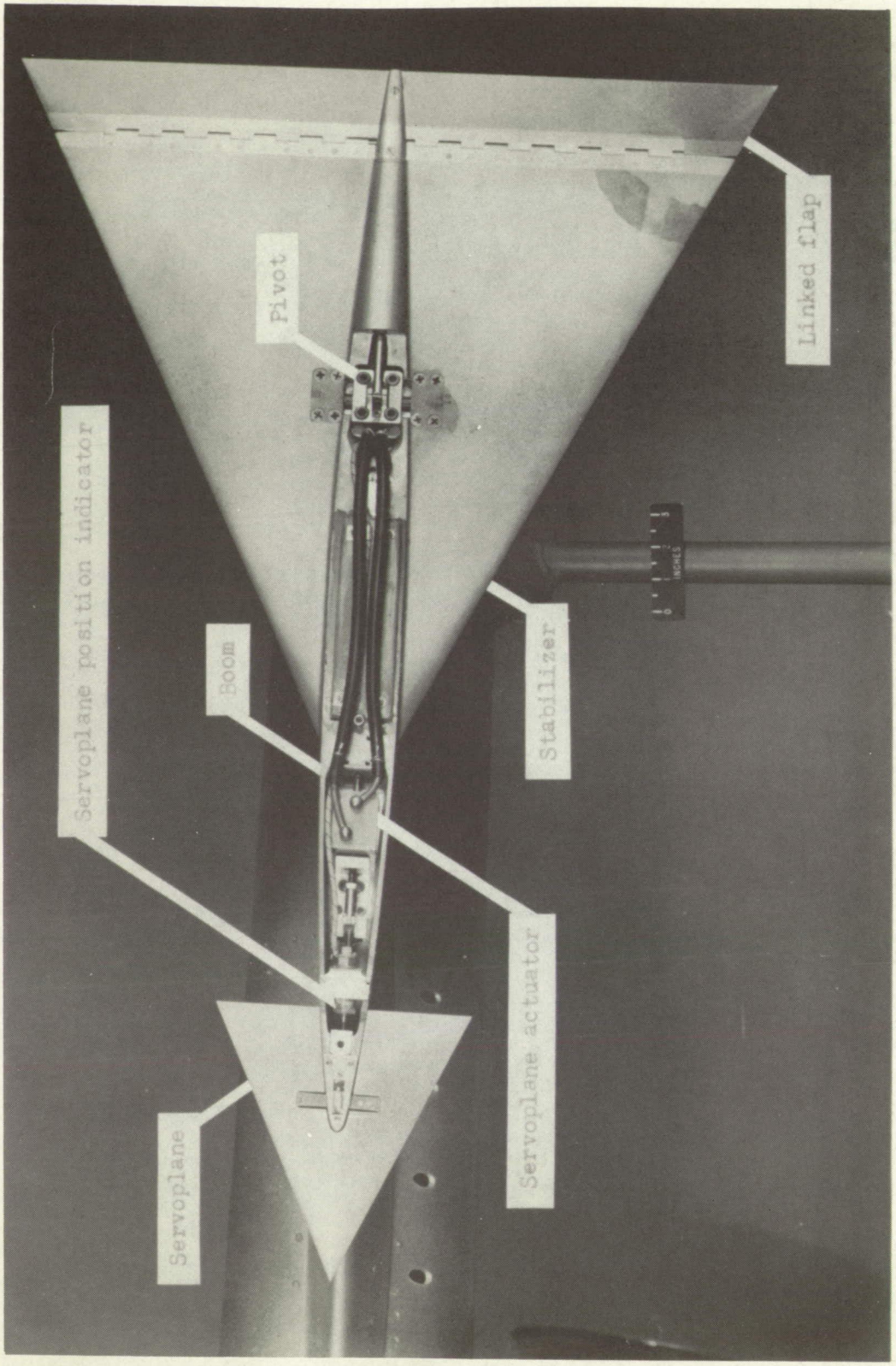

L-71243

Figure 4.- Horizontal tail with boom-hatch cover removed.

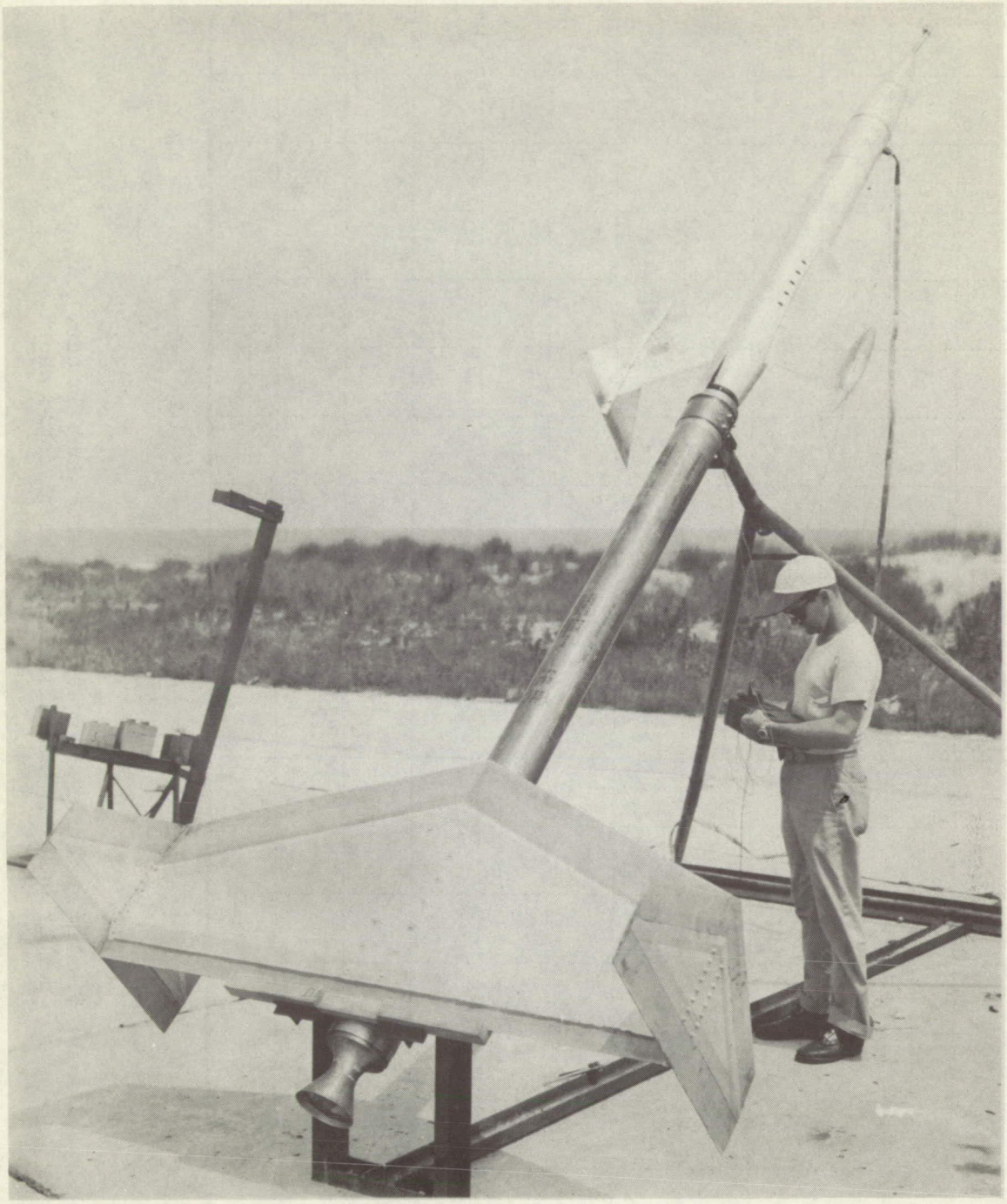

L-71564.1

Figure 5.- Rocket model B in combination with its booster rocket mounted on the launching platform.

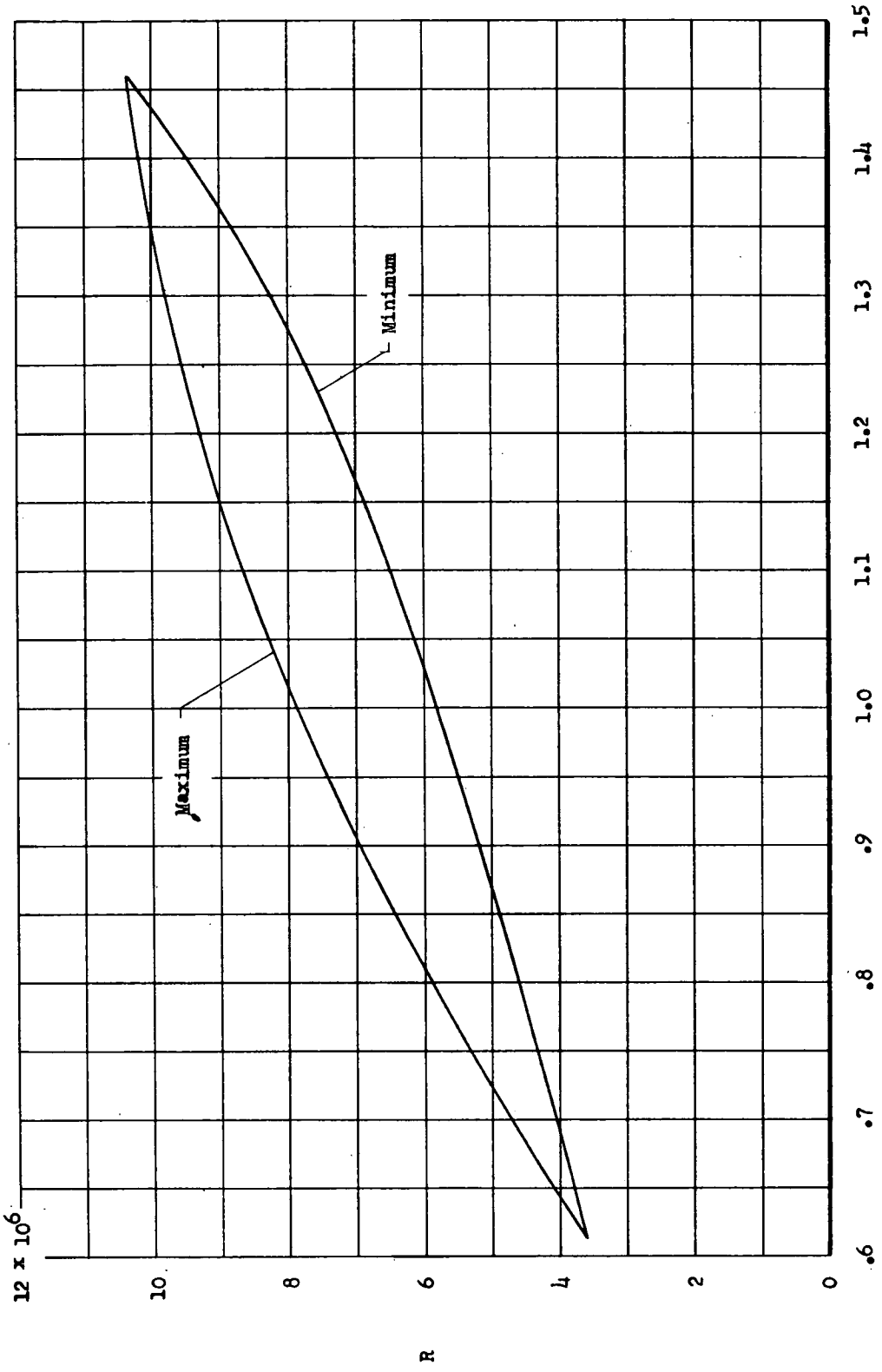

Figure 6.- Variation of Reynolds number with Mach number. Reynolds number based on stabilizer mean aerodynamic chord.

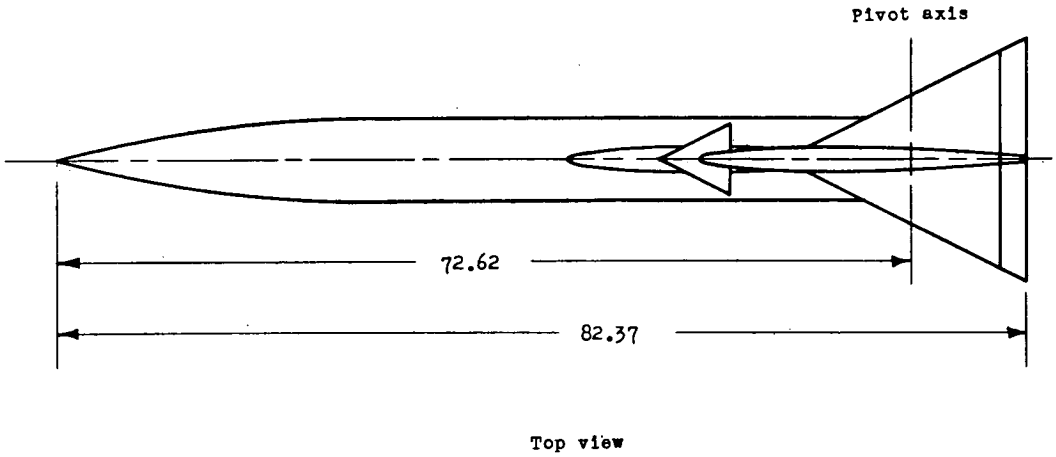

Top view

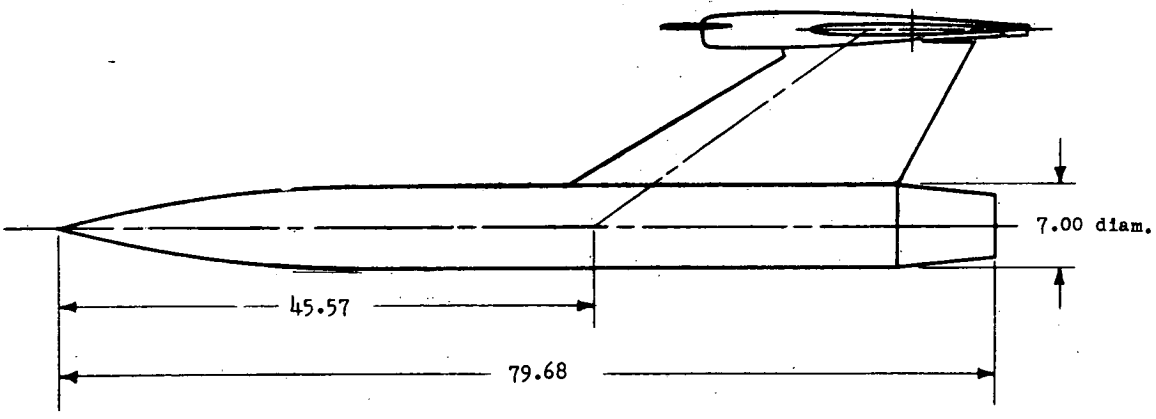

Side view

Figure 7.- General arrangement of wind-tunnel model. All dimensions are in inches.

(a) View upstream. L-67206

(b) View downstream. L-67207

Figure 8.- Wind-tunnel model mounted in the Langley stability tunnel.

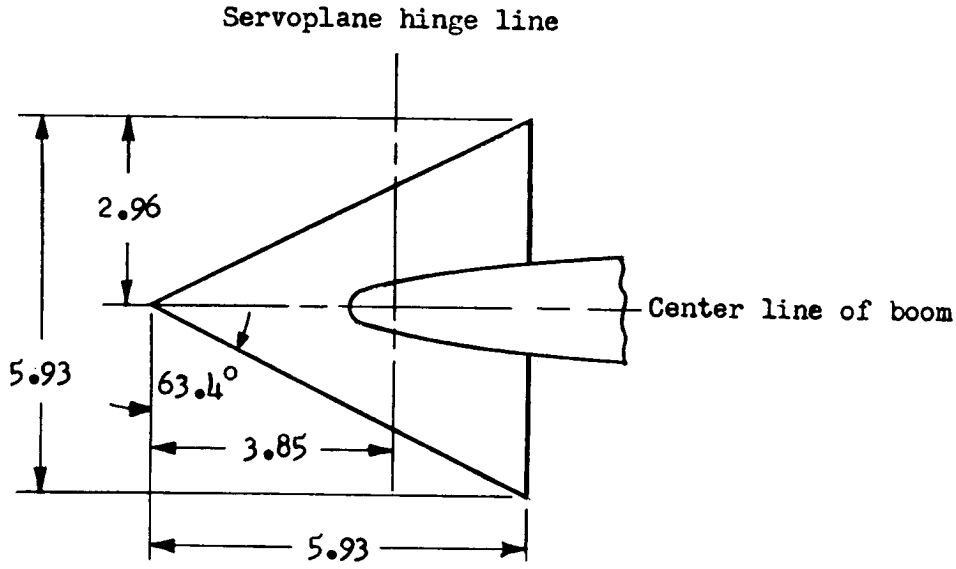

Original servoplane

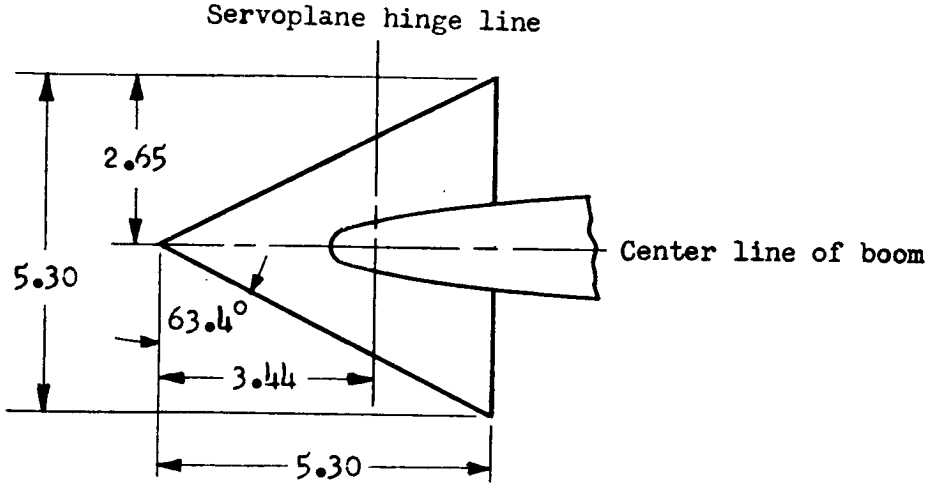

Small servoplane

Figure 9.- Plan form of original and small servoplanes. All dimensions are in inches.

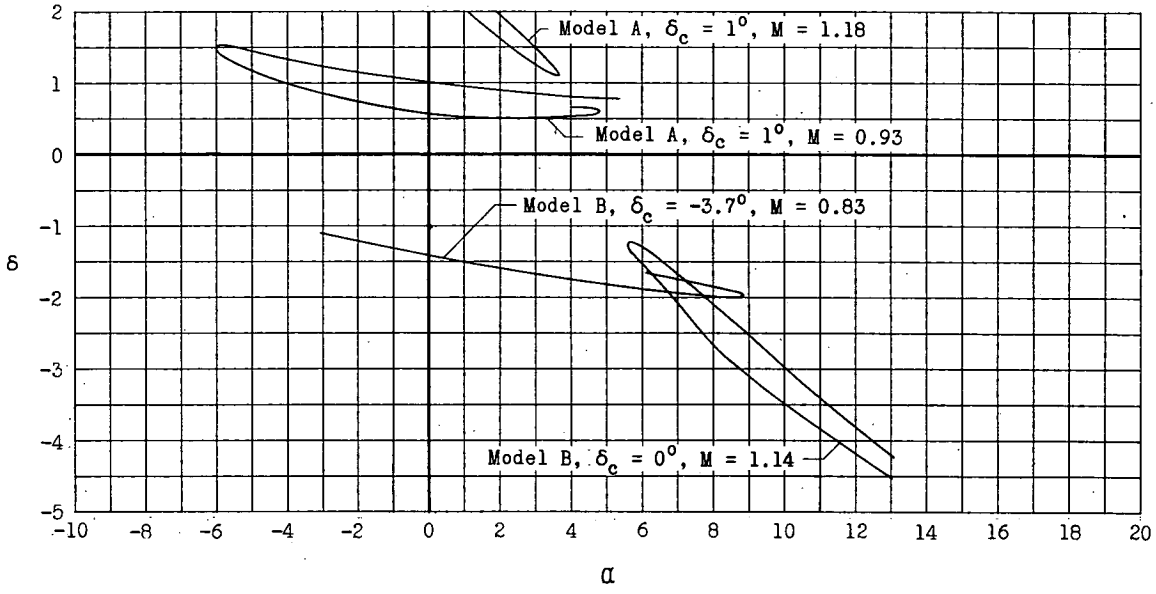

Figure 10.- Typical plots of the variation of horizontal-tail deflection with angle of attack of rocket model.

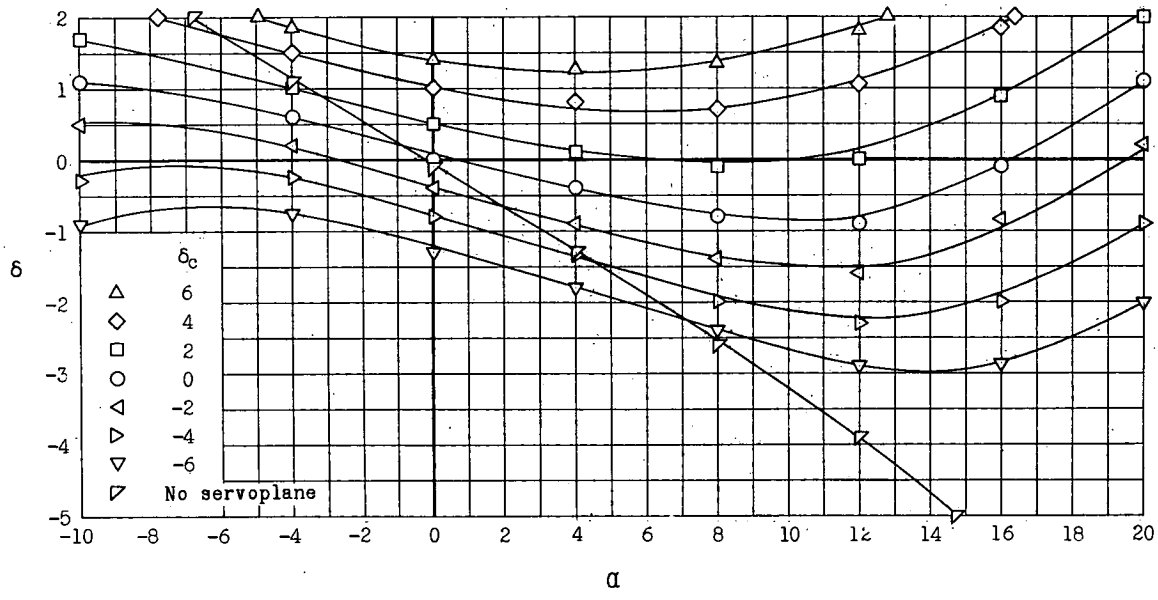

Figure 11.- Variation of horizontal-tail deflection with angle of attack at constant values of servoplane deflection as obtained from low-speed wind-tunnel tests of the original configuration.

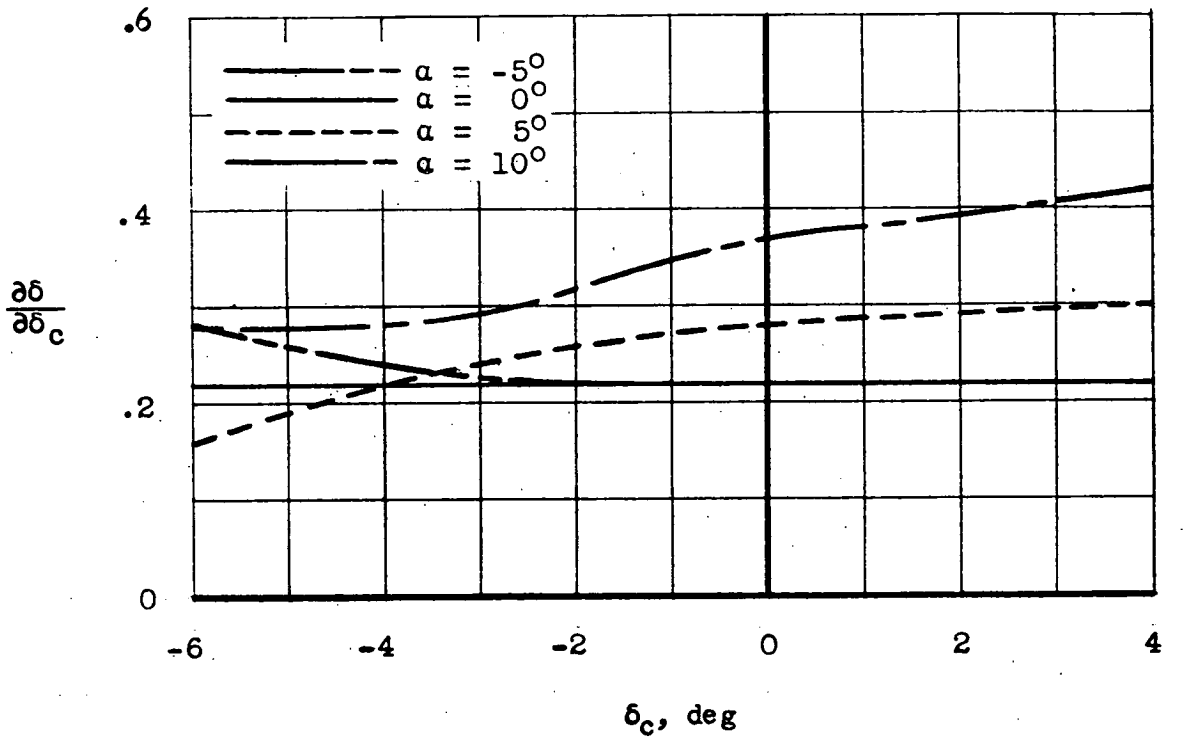

(a) Original configuration.

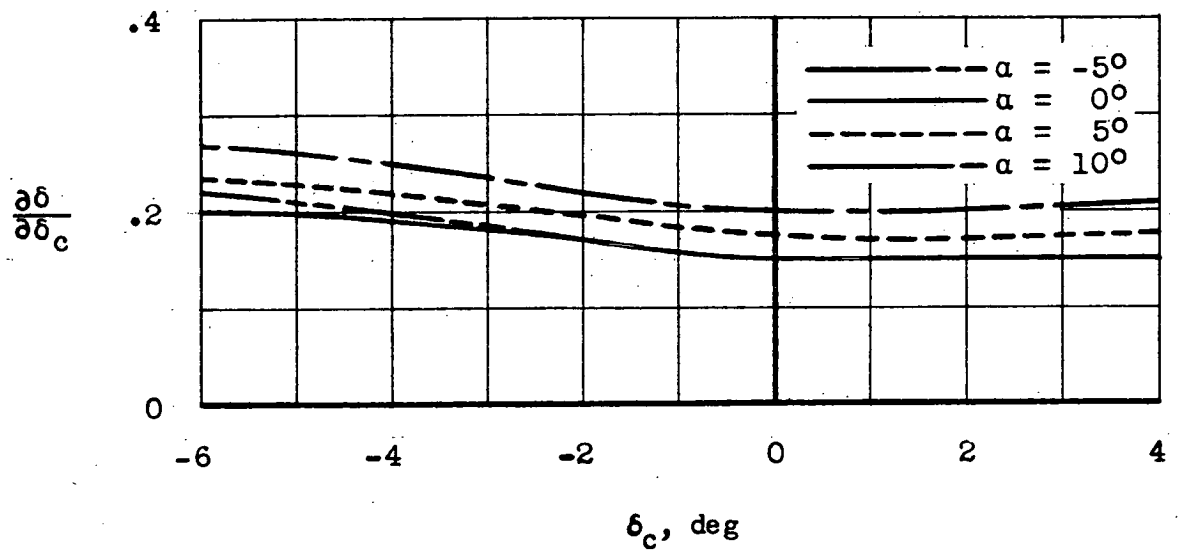

(b) Small servoplane.

Figure 12.- Variation of $\partial\delta/\partial\delta_c$ with servoplane deflection at constant angles of attack as obtained from wind-tunnel tests.

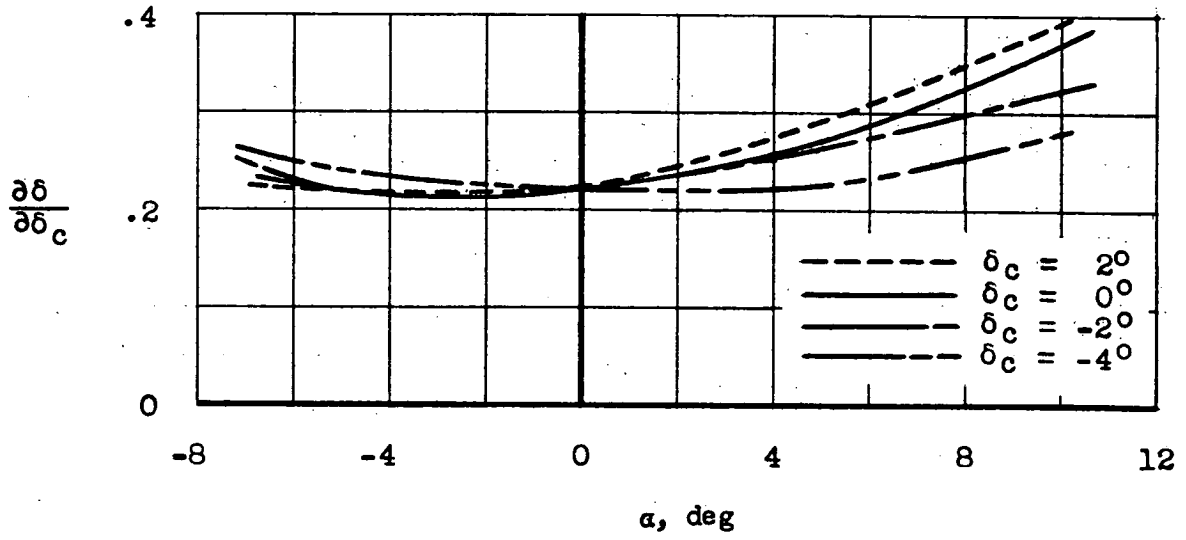

(a) Original configuration.

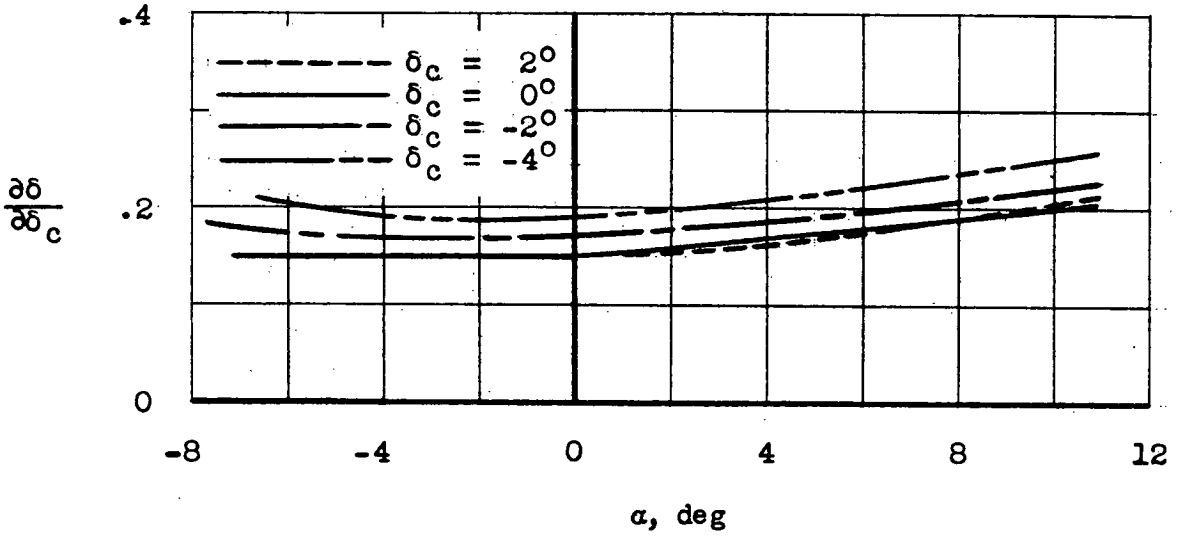

(b) Small servoplane.

Figure 13.- Variation of $\partial\delta/\partial\delta_c$ with angle of attack at constant servoplane deflection as obtained from wind-tunnel tests.

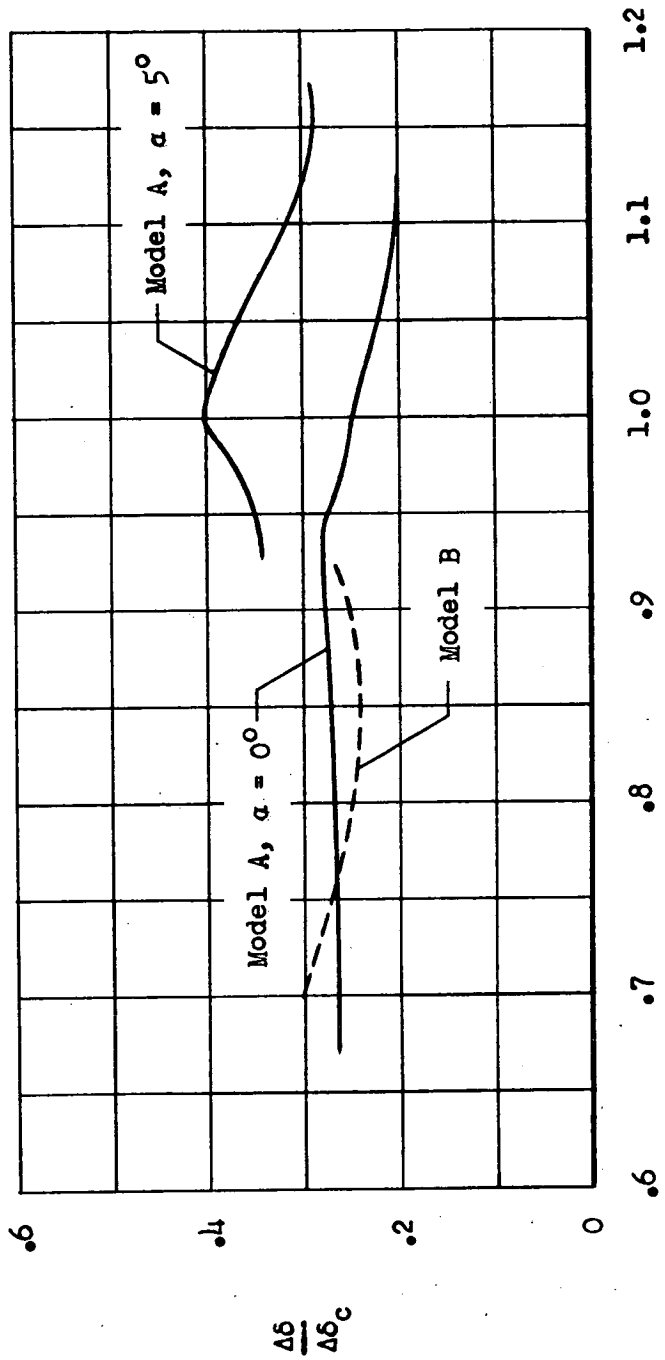

Figure 14.- Variation of servoplane effectiveness with Mach number as obtained from rocket-model tests.

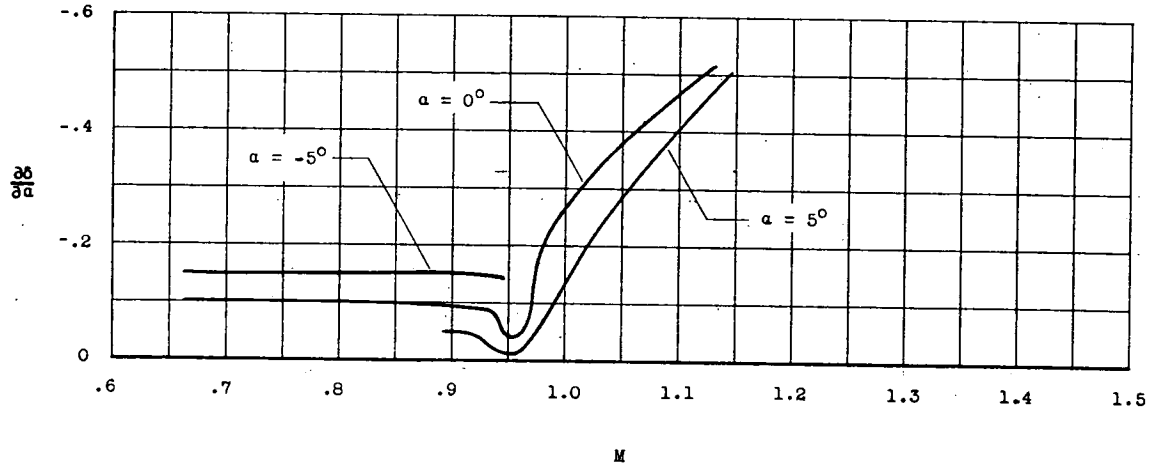

(a) Rocket model A; $\delta_c = 1^\circ$.

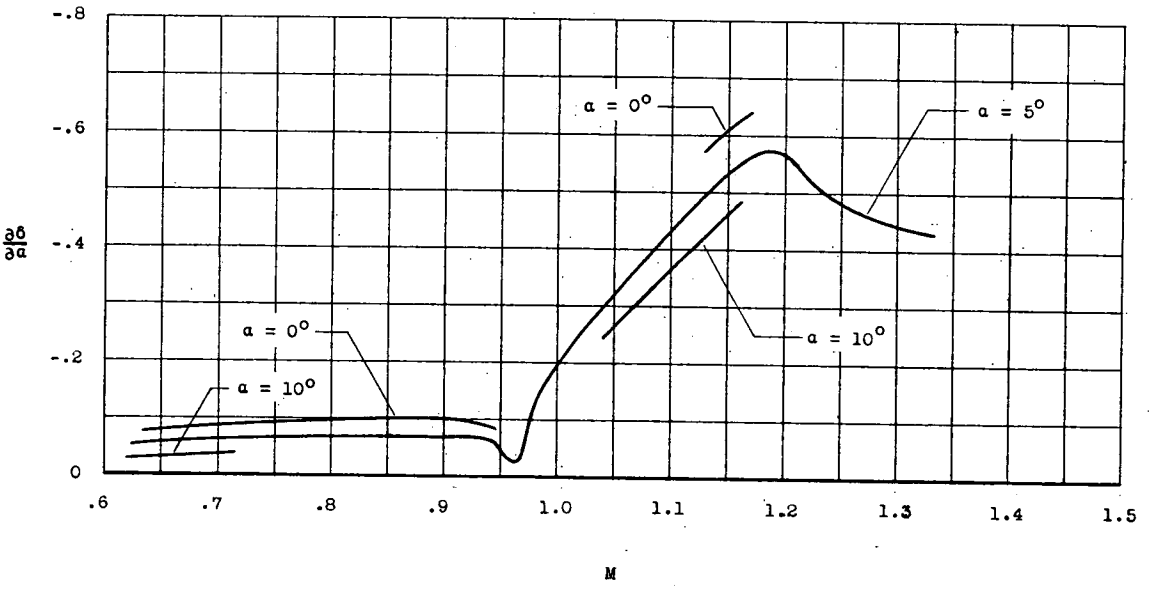

(b) Rocket model B; $\delta_c = 0^\circ$.

Figure 15.- Variation of $\partial\delta/\partial\alpha$ with Mach number at constant angles of attack as obtained from rocket-model tests.

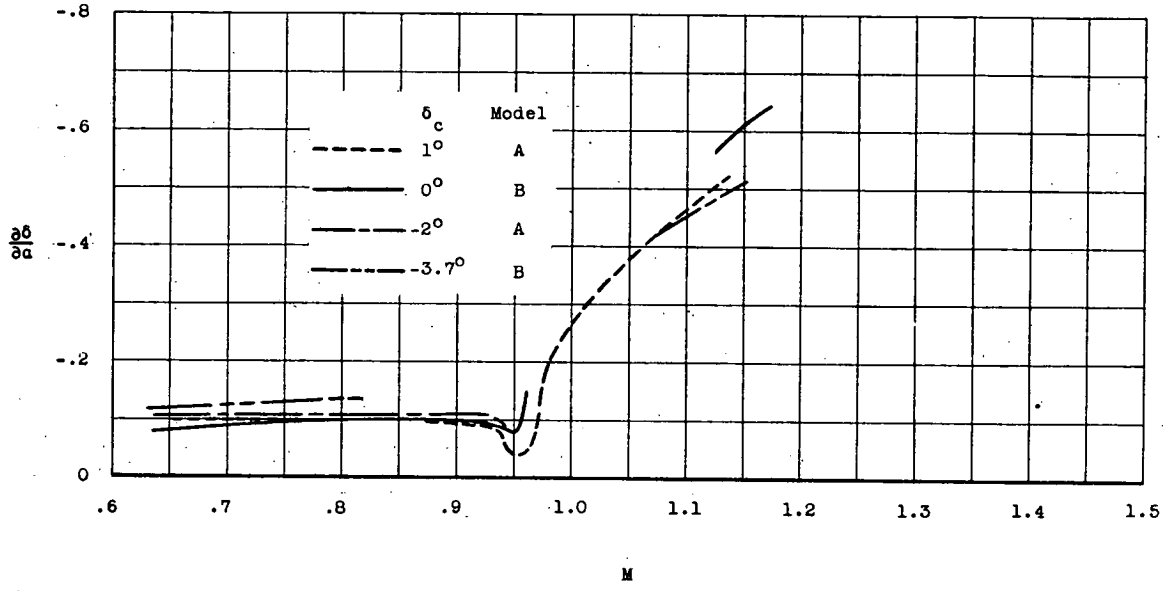

(a) $\alpha = 0^\circ$.

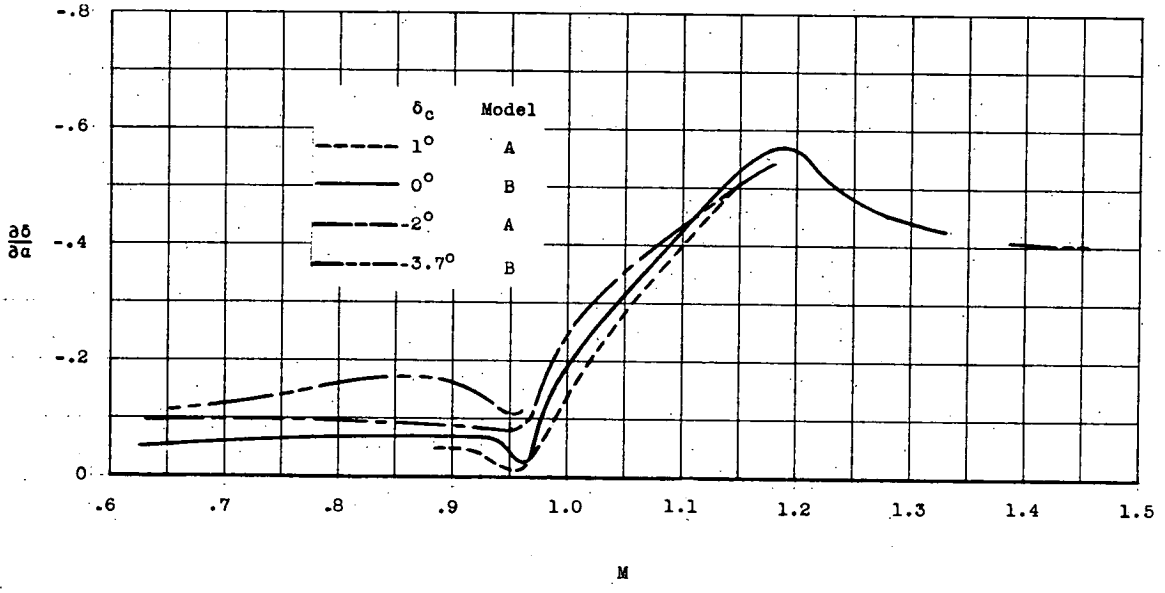

(b) $\alpha = 5^\circ$.

Figure 16.- Variation of $\partial\delta/\partial\alpha$ with Mach number at constant angles of servoplane deflection as obtained from rocket-model tests.

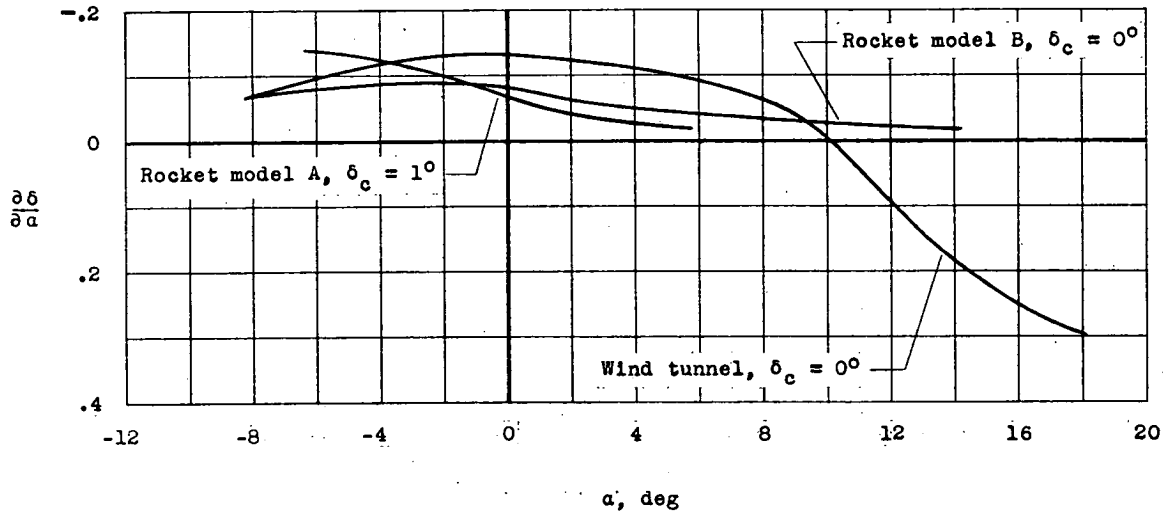

Figure 17.- Variation of $\partial\delta/\partial\alpha$ with angle of attack at constant values of servoplane deflection as obtained from rocket-model and wind-tunnel tests at subsonic speeds.

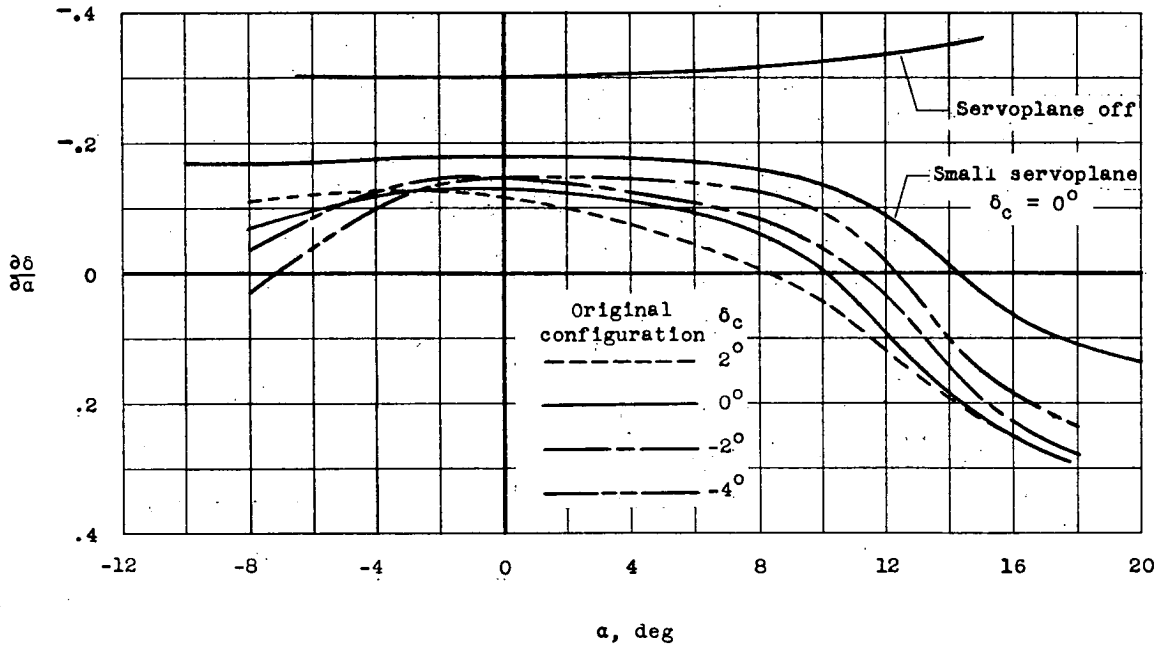

Figure 18.- Variation of $\partial\delta/\partial\alpha$ with angle of attack at constant values of servoplane deflection as obtained from wind-tunnel tests with servoplane on and off and with small servoplane.

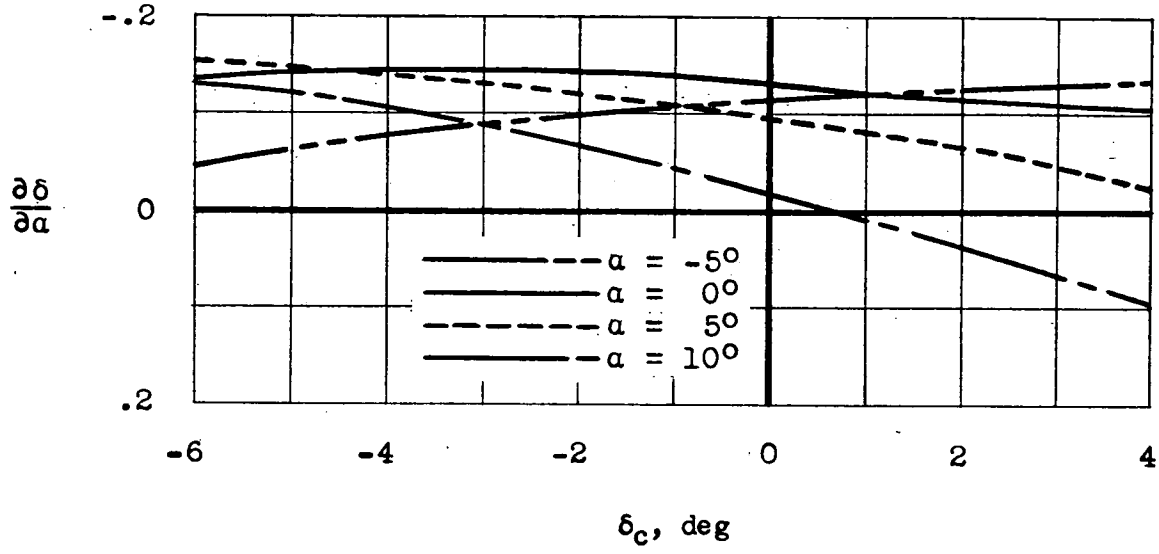

(a) Original configuration.

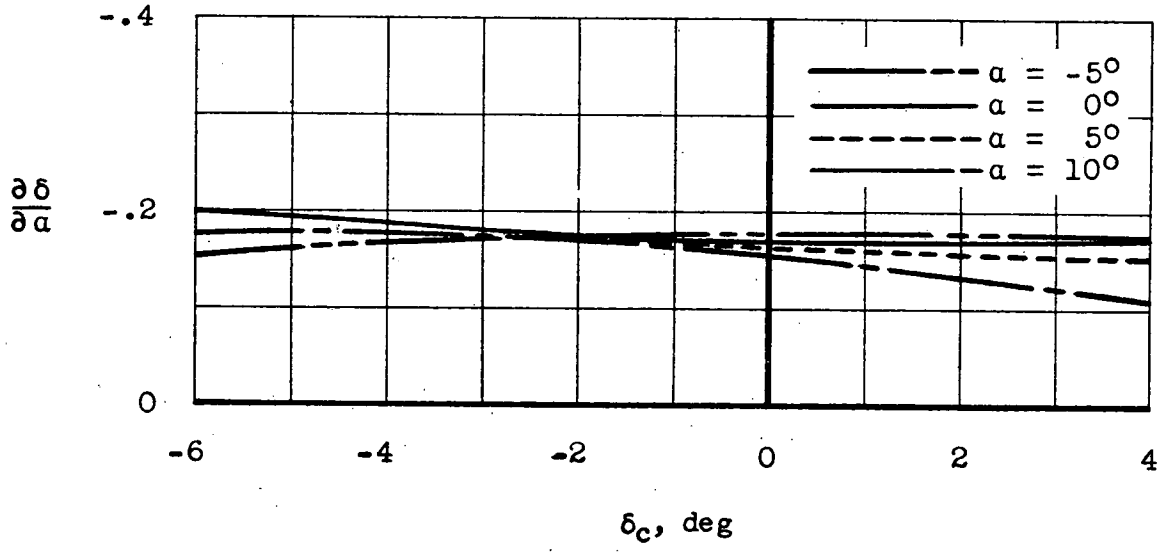

(b) Small servoplane.

Figure 19.- Variation of $\partial\delta/\partial\alpha$ with servoplane deflection at constant angles of attack as obtained from wind-tunnel tests.

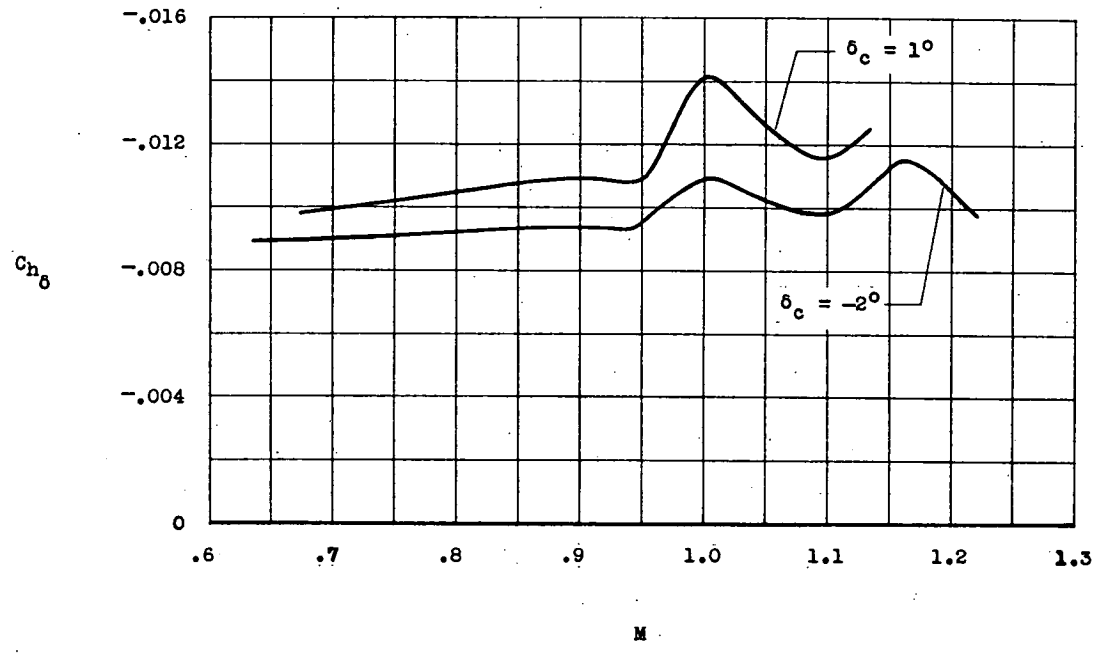

(a) Model A.

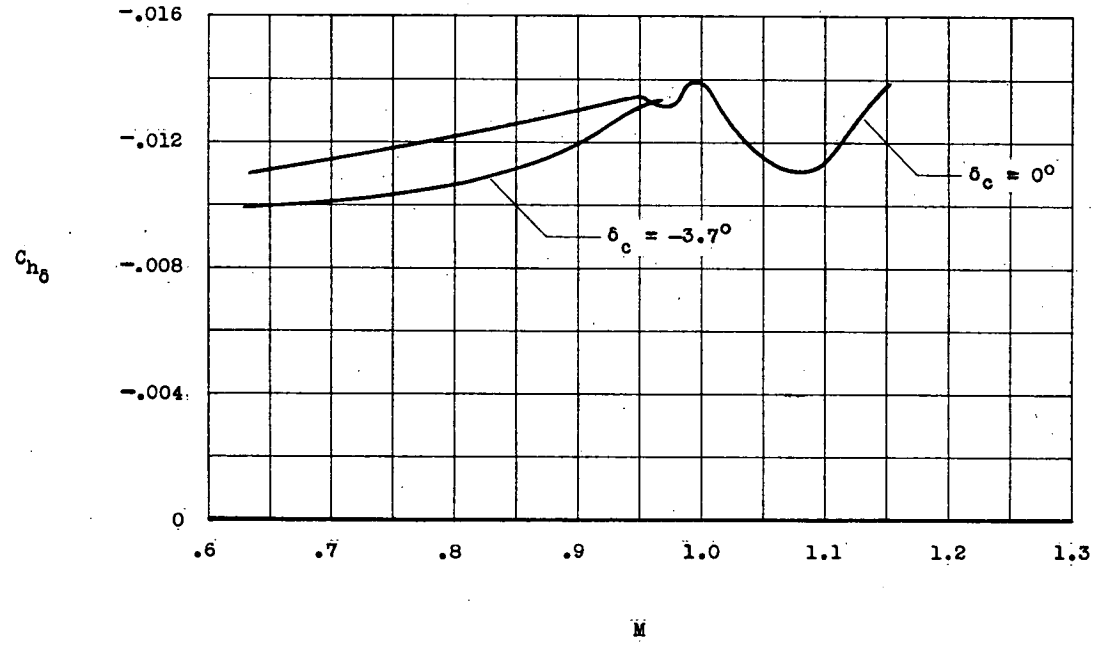

(b) Model B.

Figure 20.- Variation of horizontal-tail hinge-moment derivative C_{h_δ} with Mach number as obtained from rocket-model tests.

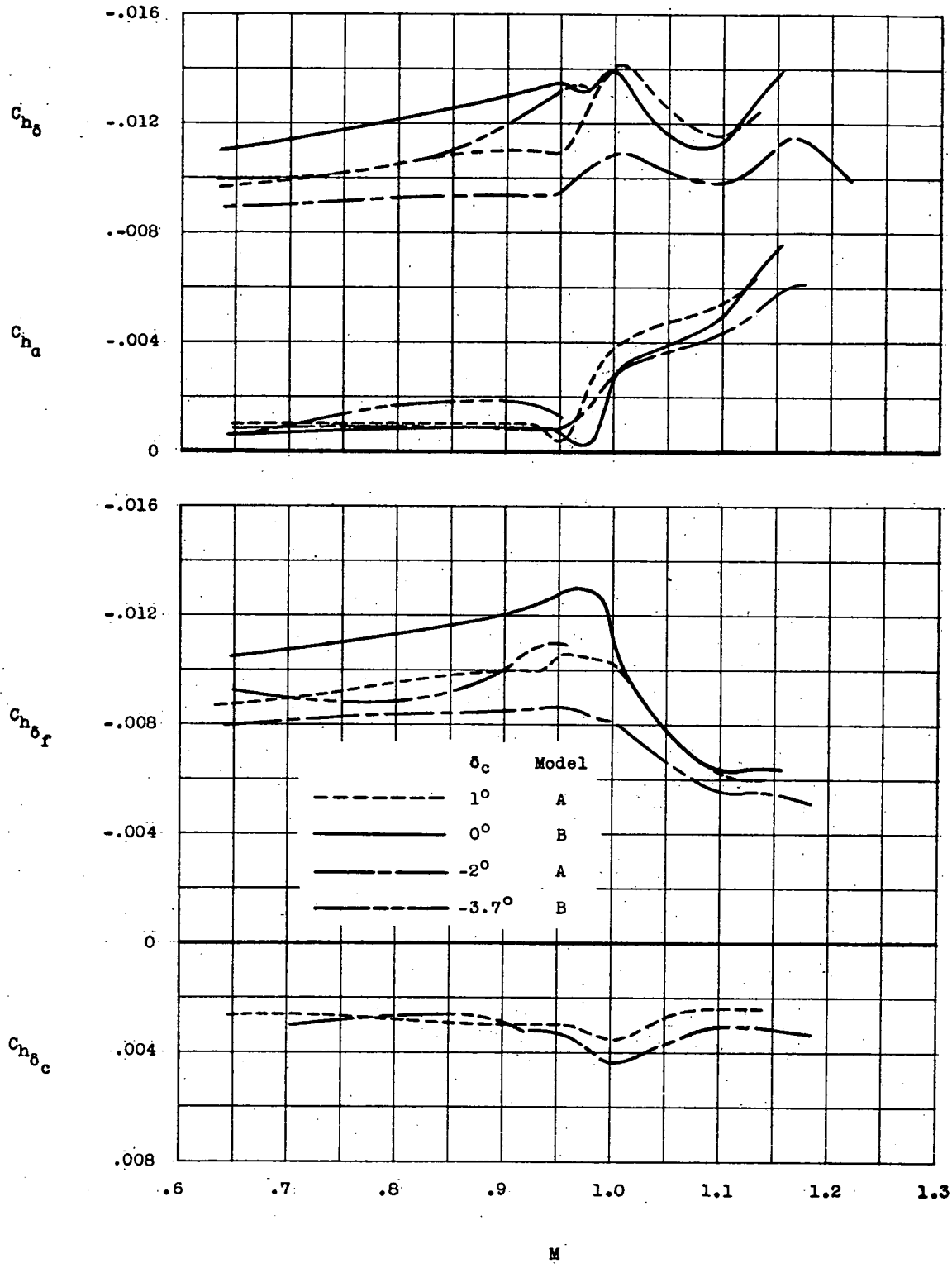

Figure 21.- Variation of horizontal-tail hinge-moment derivatives with Mach number as obtained from rocket-model tests.

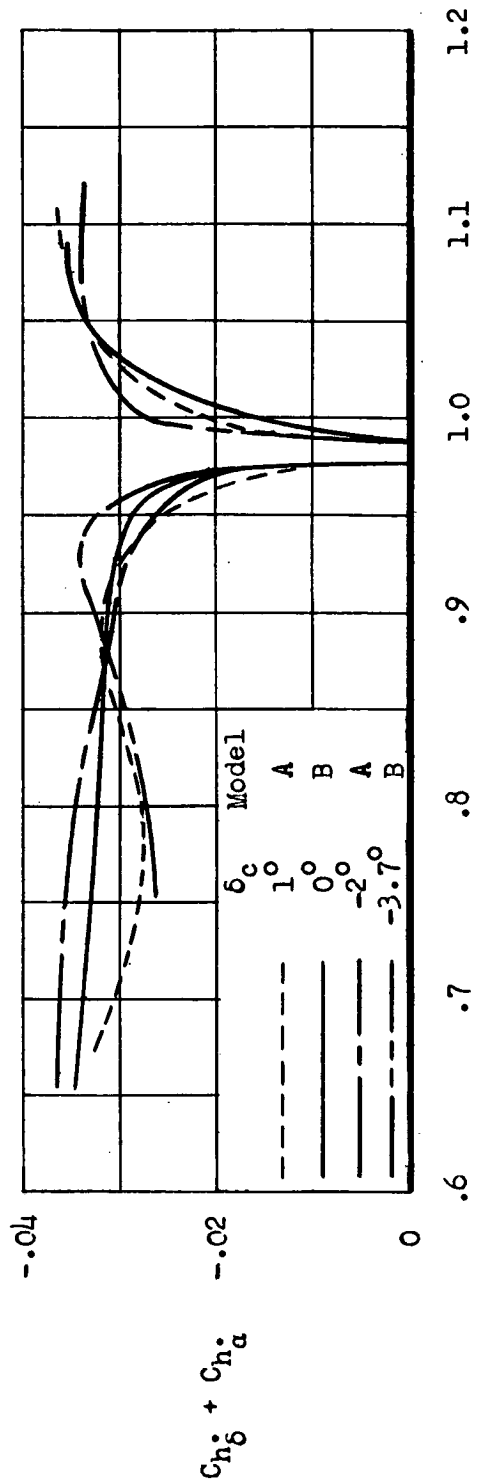

Figure 22.- Variation of horizontal-tail damping derivatives with Mach number as obtained from rocket-model tests.

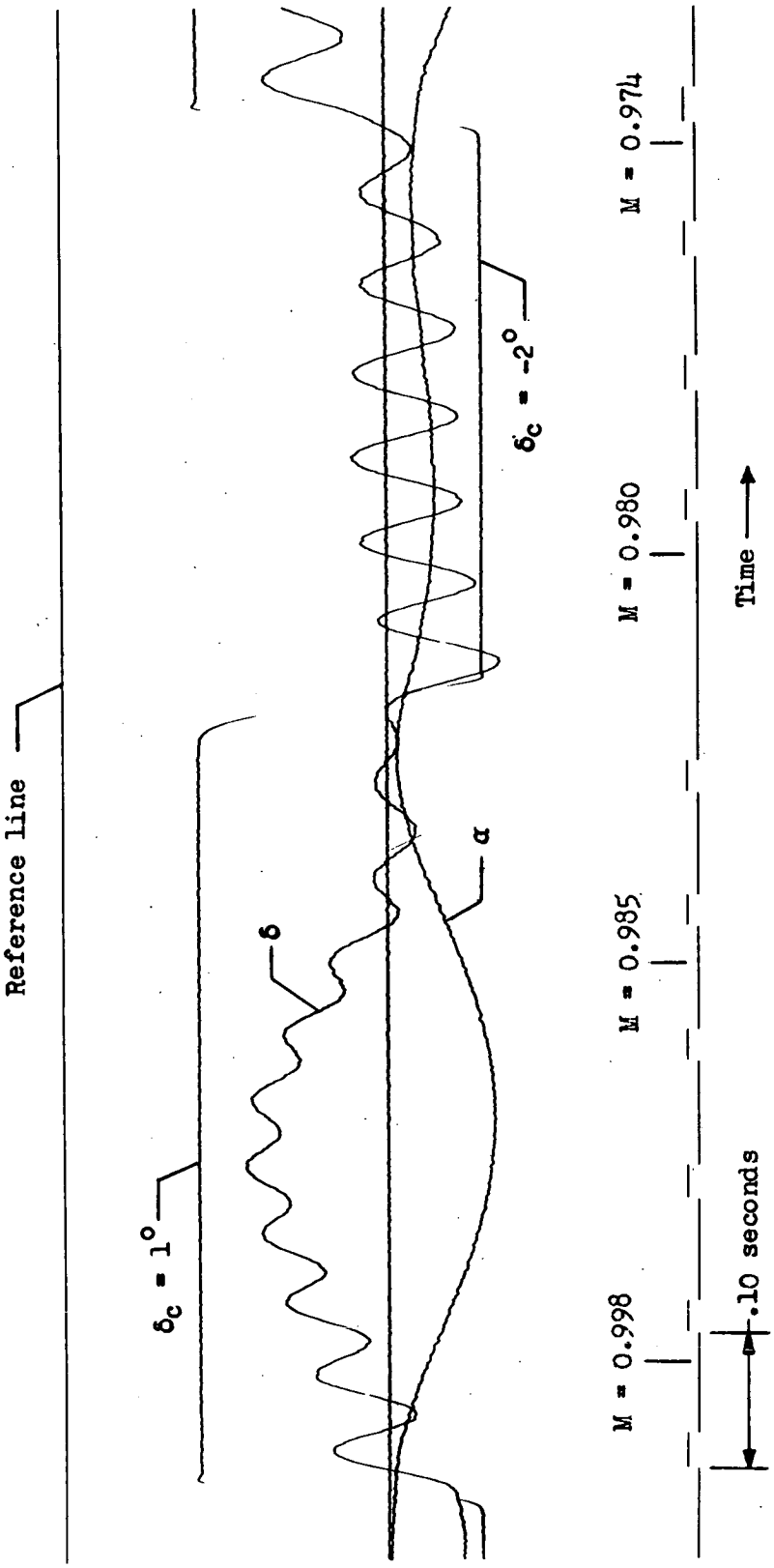

Figure 23.- Reproduction of section of telemeter record obtained from rocket model A showing dynamic instability of the free-floating horizontal tail.

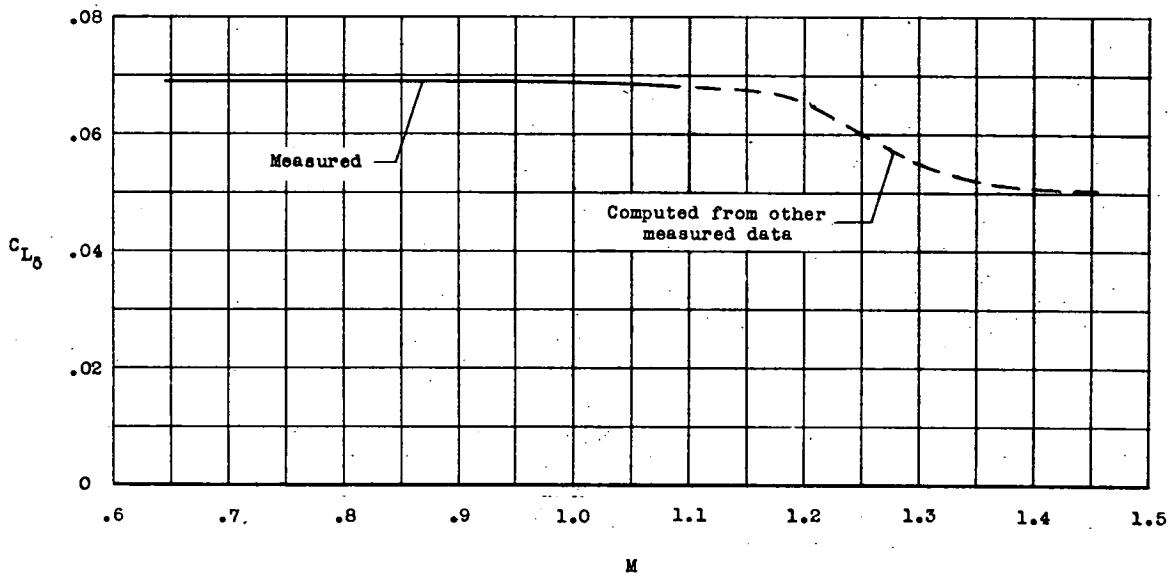

Figure 24.- Variation of lift due to tail deflection with Mach number as obtained from rocket model B.

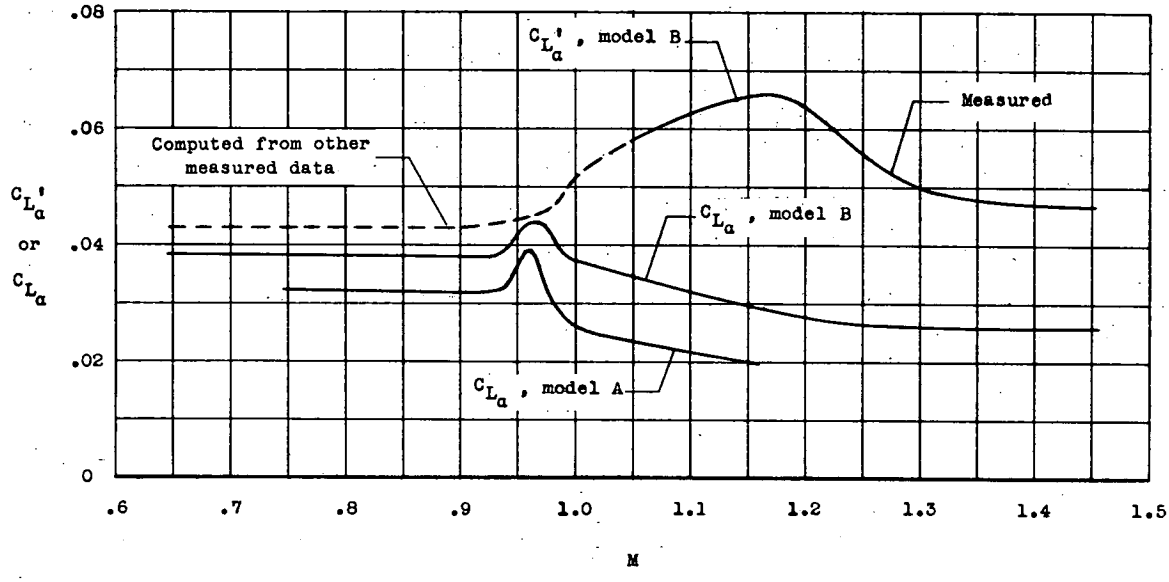

Figure 25.- Variation of lift-curve slope with Mach number as obtained from rocket-model tests with horizontal tail both free floating and fixed.

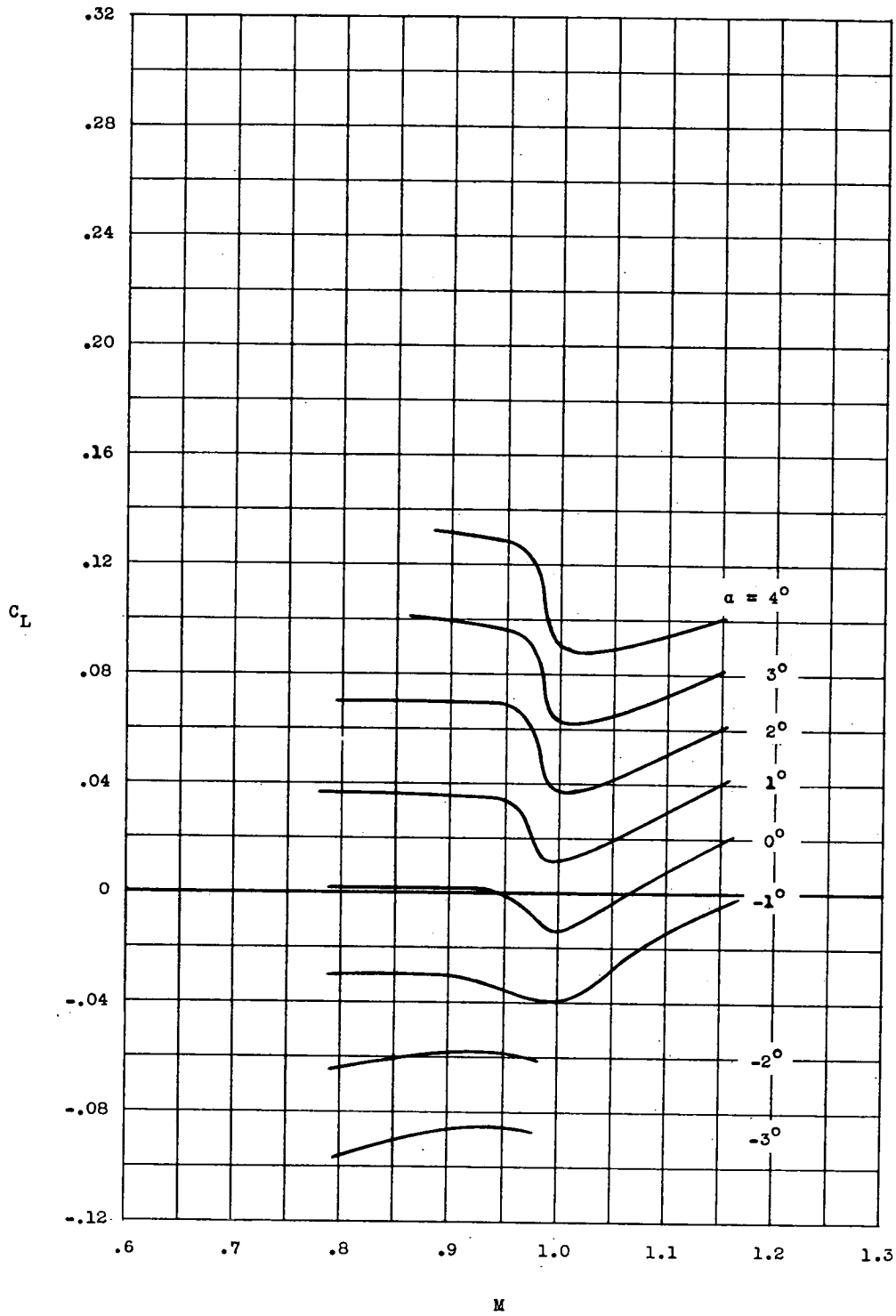

(a) Model A; $\delta_c = 1^\circ$.

Figure 26.- Variation of model lift coefficient with Mach number at constant angles of attack.

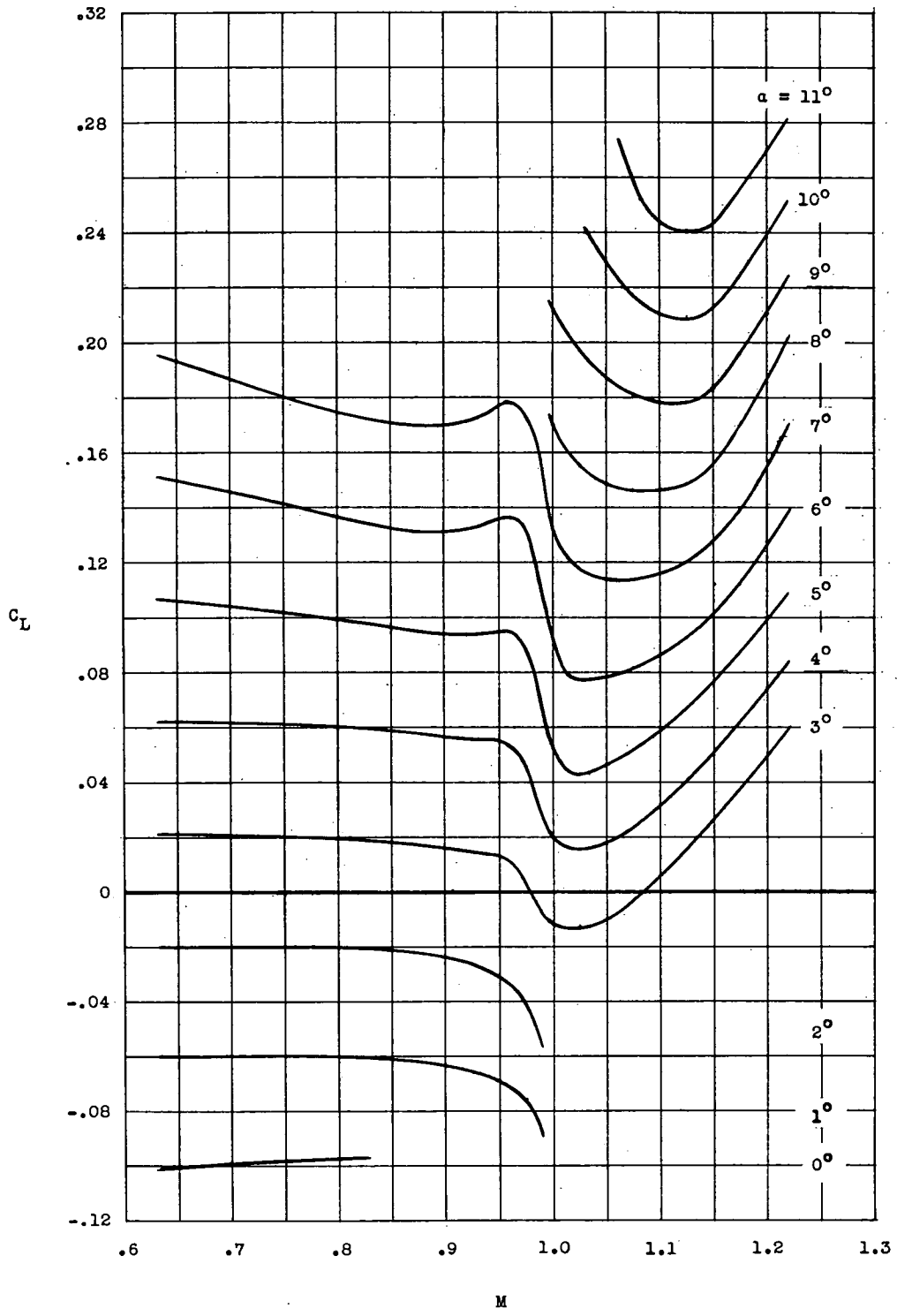

(b) Model B; $\delta_c = 0^\circ$.

Figure 26.- Concluded.

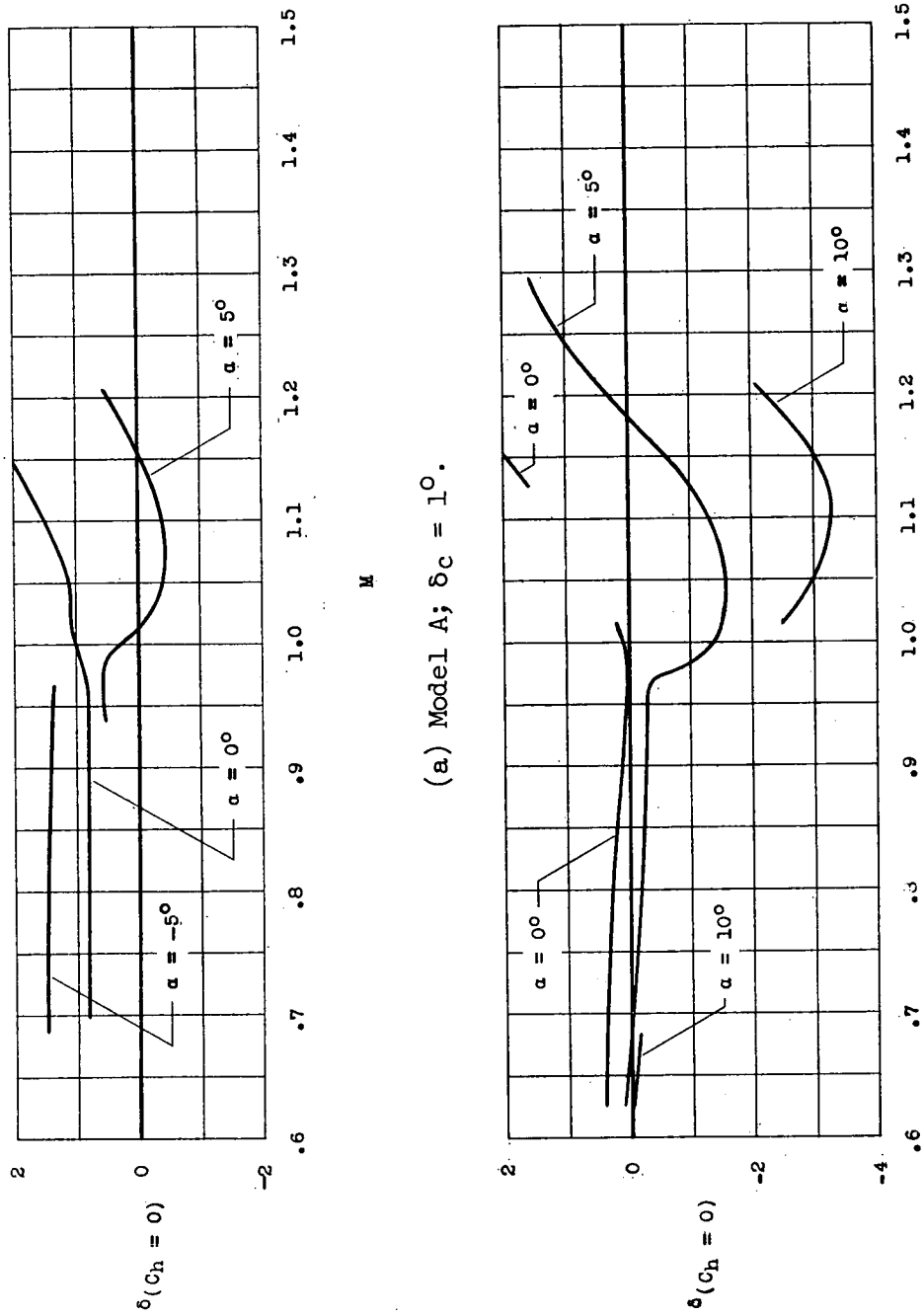

(a) Model A; $\delta_c = 1^\circ$.

(b) Model B; $\delta_c = 0^\circ$.

Figure 27.- Variation of trim horizontal-tail deflection with Mach number at constant angles of attack as obtained from rocket-model tests.

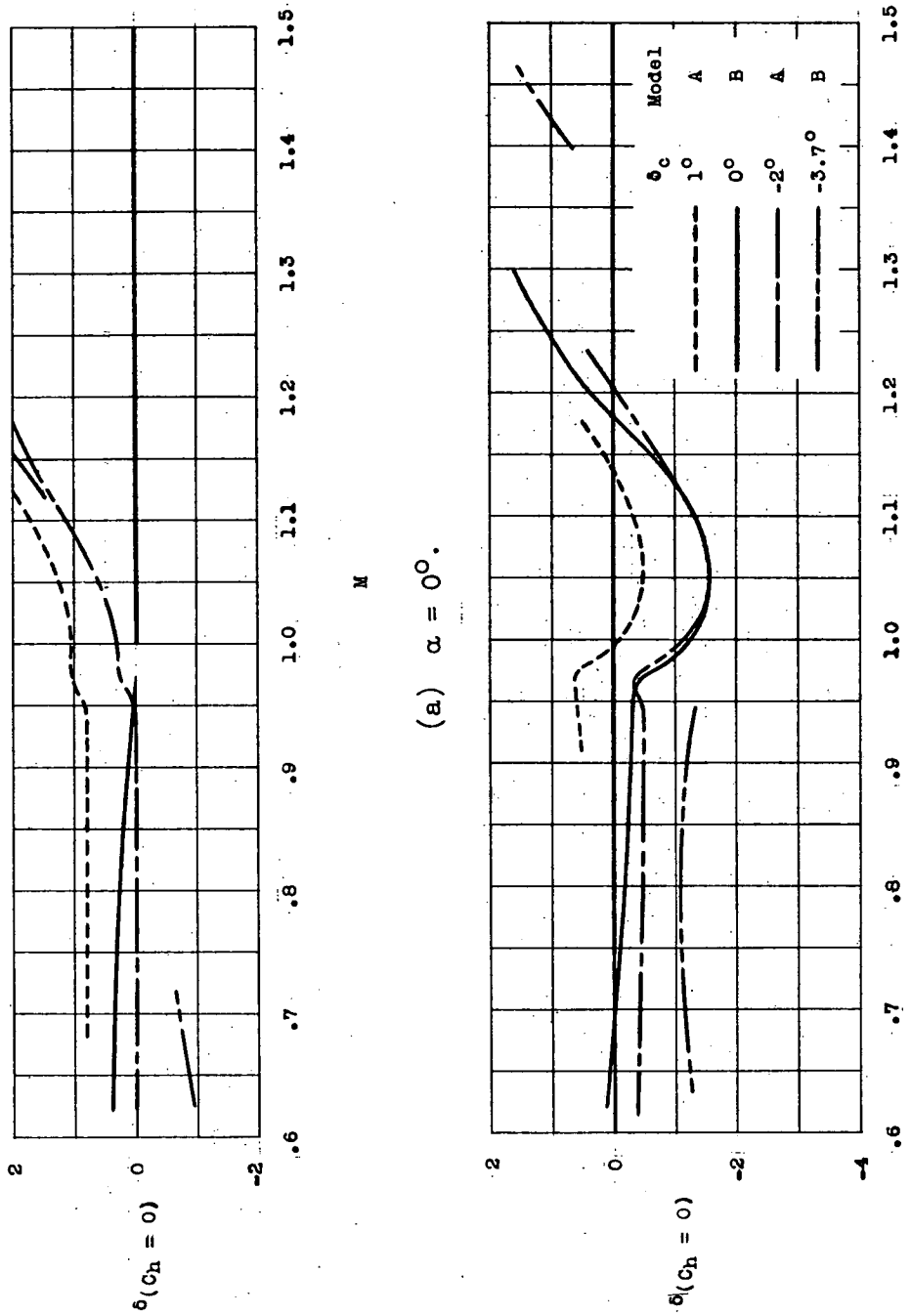

(a) $\alpha = 0^\circ$.

(b) $\alpha = 5^\circ$.

Figure 28.- Variation of trim horizontal-tail deflection with Mach number at constant values of servoplane deflection as obtained from rocket-model tests.

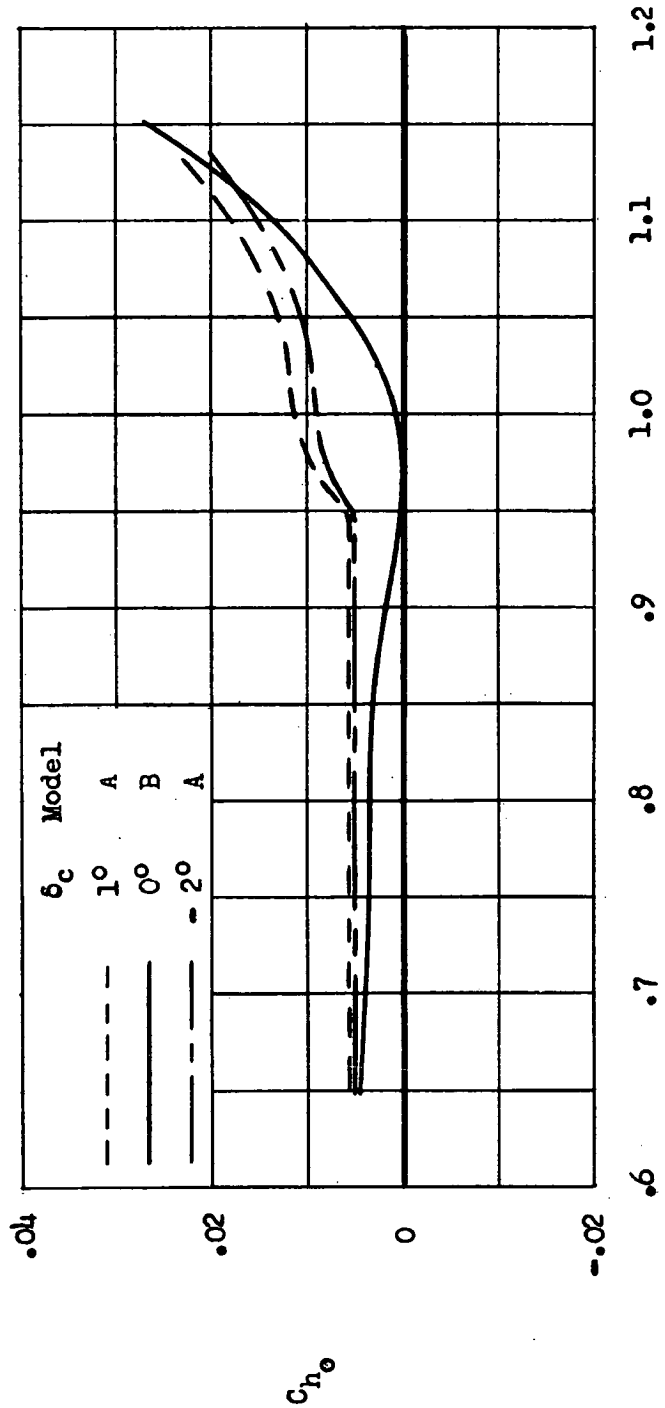

Figure 29.- Variation of basic tail hinge-moment coefficient with Mach number.

NACA-Langley - 12-4-53 - 325